Crack-tip process zone as a bifurcation problem

Alexei Boulbitch,[1,*] Yury M. Gufan,[2] and Alexander L. Korzhenevskii[3]
[1]*IEE S.A. ZAE Weiergewan, 11, rue Edmond Reuter, L-5326 Contern, Luxembourg*
[2]*Institute for Physics, Stachki 194,344090 Rostov-on-Don, Russia*
[3]*Institute for Problems of Mechanical Engineering, RAS, Bol'shoi prosp. V. O. 61, 199178 St. Petersburg, Russia*
(Received 18 March 2017; published 24 July 2017)

Stress concentration at a crack tip generates a solid structural transformation in its vicinity, the process zone. We argue that its formation represents a local phase transition described by a multicomponent order parameter. We derive a system of equations describing the dynamics of the order parameter driven by an inhomogeneous, time-dependent stress field in the solid and show that it exhibits a bifurcation. The latter corresponds to the emergence of a process zone characterized by the distribution of the order parameter localized in the vicinity of the crack tip. The emergence temperature T_* considerably differs from the temperature of the bulk phase transformation T_c. We demonstrate that T_* exhibits a universal behavior $T_* - T_c \sim K_I^{4/3}$, in terms of the stress intensity factor K_I, and that the zone universally vanishes upon achieving a critical velocity. These facts together give rise to a universal dynamic phase diagram.

DOI: 10.1103/PhysRevE.96.013005

I. INTRODUCTION

It is common knowledge that high stresses $\sim 10^9$ to 10^{11} Pa concentrate at the tips of brittle cracks. The stress slowly decreases with distance according to the $r^{-1/2}$ law, where r is the distance measured from the tip. Such a stress level is great enough to alter some physical or chemical properties of the material. This results in the crack tip's being surrounded by a small, nanometer to micrometer sized *process zone*, the region where at least some material properties differ from those in the bulk. This is not surprising since a glance at the phase diagrams [1] shows that even a moderate hydrostatic pressure in most solids gives rise to crystal structure reconstructions. One should expect, therefore, that such a level of tensile and shear stress at the crack tip also gives rise to phase transformations in its vicinity, although eventually different from those generated by hydrostatic pressure [1]. In this case, the process zone represents a small region of a *daughter* phase embedded in the bulk *mother* phase (as is schematically shown in Fig. 1). The latter is stable in the bulk of the solid, while the former is only stabilized by the stress in the close vicinity of the crack tip. The variation of the physical properties within the process zone is a direct consequence of such a local phase transformation. In this paper, such a zone will be referred to as the *transformational process zone*.

It is commonly believed that the process zone is responsible for the formation of both the threshold of the crack stability K_{IC} as well as the dynamic resistance to its growth. This opinion has spurred an interest in the mechanisms underlying these phenomena. For a long time, however, transformational process zones have only been experimentally analyzed in a "post mortem" way: a thin layer of a daughter phase has been discovered in some materials on the fracture surfaces of broken samples [2,3]. Such post mortem observations are only possible, provided that (i) the mother to daughter phase transition is of the first order, and (ii) the solid is deeply in the hysteresis region of its phase diagram. In the latter case, the daughter phase is metastable and may survive a certain time before decaying. In most solids, the width of the hysteresis region is, however, small ($\sim$1 K) [1,4] compared to the overall phase diagram width of the domain of the solid phase existence, between a few hundred and a few thousand degrees [1]. For this reason, in most cases the material appears to be *outside* of the hysteresis region of the nearest bulk phase transitions during measurements. This explains the rarity of reports of the post-mortem detection of a transformational process zone.

This situation has changed during the last decade with the implementation of new experimental techniques. This has enabled the study of transformational process zones in detail, often down to the fine structure, sometimes even allowing doing this *in situ*. The direct imaging of the atomic locations by high-angle annular dark-field scanning transmission electron microscopy (TEM) [5], electron nanodiffraction [6], a micromechanical loading combined with *in situ* high-resolution x-ray microdiffraction [7], an *in situ* scanning electron microscopy (SEM) combined with electron backscatter diffraction [8], an *in situ* digital image correlation technique [9], Raman mapping [10], and atomic force microscopy [11,12]; this is an incomplete list of the experimental approaches enabling one to study the process zones.

The above methods, together with the more traditional ones [3], have revealed that the solid structure in the close vicinity of the tip indeed undergoes chemical and/or structural reconstructions. They have, as well, enabled one to resolve the structure of the process zone.

The observation of the transformational process zone at the tip of a crack has been reported in a number of metals and alloys [6,8,13–16] as well as in dielectrics [2,3,10,17], superconductors [18], and polymers [19–21]. These observations reveal a great variety of crystal structures of the transformational process zones in materials of different sorts, suggesting that formation of such a process zone is a typical phenomenon exhibiting universal features. Observations of the temperature dependence of the size of the process zone [22] as well as its emergence at $\Delta T_* = T_* - T_c \approx 300$ K away from the line of the bulk phase transition T_c [23] suggests that, at least in some materials, the emergence of a process zone has the

*Corresponding author: alexei.boulbitch@t-online.de

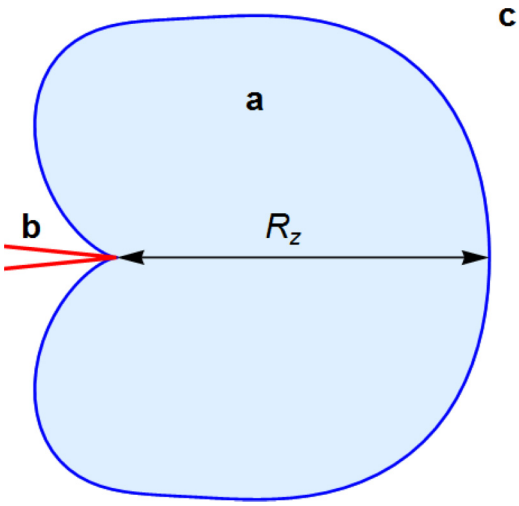

FIG. 1. Schematic view of the process zone (a) with the size R_Z located at the crack tip (b) and embedded in the mother phase matrix (c).

character of a bifurcation: it emerges at some temperature T_* away from the temperature of the bulk phase transformation T_c, and, further, its size gradually increases when the temperature approaches T_c.

In theoretical descriptions of the process zone, one can distinguish three approaches. On the one hand, atomistic mechanisms of the formation of the zone have been studied by computer simulations [6,24–33].

On the other hand, an analytical, continuum mechanical approach has been developed. It is based on the assumption that the transformational process zone only differs from the rest of the solid by its (i) elastic moduli and (ii) the spontaneous strain caused by the phase transformation. This approach describes the zone solely by the configuration (and, eventually, dynamics) of its interface as well as the stress or strain distribution, while all other degrees of freedom are ignored. The reviews describing this approach can be found in [2,3,34]. We develop a third approach. We take a new view of the process zone, as a small domain at the crack tip whose properties differ qualitatively from those in the bulk. This difference is closely related to the behavior of a set of internal degrees of freedom of the solid responsible for the phase transformation. By analogy with the Landau theory of phase transitions [35], this set is referred to as the *order parameter*. The numerical description of the process zone within such an approach has been addressed in [36–39].

The possibility of applying this approach analytically has been indicated in [40] and described in detail in [39] within a model with a one-component order parameter. The paper [41] employed this model to describe a self-oscillation of the crack propagation generated by the energy dissipation within the process zone. In [38,42], we predicted crack velocity jumps engendered by a process zone described by a one-component order parameter.

However, most phase transitions cannot be adequately described by a simple one-component order parameter, and a multicomponent order parameter is absolutely required [43,44].

To give the reader an idea of the occurrence in nature of order parameters with different dimensionalities n, we provide here a few examples. There are a number of materials exhibiting phase transformations described by a one-component order parameter. It is, for example, the case for the strongly anisotropic magnetics, such as K_2CoF_4, Rb_2CoF_4, and others [45]. A one-component order parameter also describes the paraelectric to ferroelectric transitions in uniaxial dielectric ferroelectrics, such as $LiTiO_3$, $LiNbO_3$, K_2PO_4, Pb_5GeO_{11}, triglycine sulfate $(NH_2CH_2COOH)_3H_2SO_4$, and some others [46]. It also controls the transitions in ferroelectrics-semiconductors, such as SbSJ [46], in binary bcc alloys, such as Fe-Be [47] and CuZn [35], and describes the α-β transition in quartz [48].

The transition between the normal and superconductive phases taking place at low temperatures in conventional superconductors, such as is described by a wave function of the superconducting condensate which represents a two-component complex scalar. It can be reduced, however, to a one-component order parameter after elimination of the Goldstone mode [49]. Such properties exhibit Sn, Pb, Fe, etc. [1], Nb and Ta [50], superconductive compounds, such as C_6Ca [51] and $C_{60}K_3$ [52], and many others.

The transitions in layered magnetics K_2MnF_4, $BaMnF_4$ [45] as well as in ferroelectrics K_2SeO_4 [53], gadolinium molybdate $(Gd_2Mo_3O_{12})$ [54], calomel (Hg_2Cl_2) [55], perovskite $CsPbCl_3$ [56], and in $PrMn_2O_5$ [57] are described by an order parameter with its number of components $n = 2$.

The magnetic phase transitions in classical ferromagnetics Fe, Ni, Co, in ferromagnetics $Tb_{1-x}Ho_xFe_2$ and $Tb_{1-x}Dy_xFe_2$ [58], the antiferromagnetic $RbMnF_3$, in the ferroelectric transitions in $BaTiO_3$, $PbTiO_3$, the structural phase transitions in $SrTiO_3$, $KMnF_3$, $LaAlO_3$ [46], PZT $[Pb(Zr_xTi_{1-x})O_3]$ [59], in binary fcc alloys such as Al-Li [60], in a number of Ni-based ones [47], and in many other materials, are described by three-component order parameters.

The magnetic phase transitions in $CeAl_2$ [61], in MnO [62], in the rare-earth metals Ho, Dy, Tb [63], type II antiferromagnets TbAs, TbP, TbSb, $TbAu_2$, and NbO_2 [64], structural transitions in VO_2 [43,65], in langbeinites, such as $RbCd_2(SO_4)_3$ as well as the transitions into a superconductive phase in the unconventional superconductors, such as Sr_2RuO_4 [66], are described by four-component order parameters.

Type I antiferromagnet UO_2, type III antiferromagnet K_2IrCl_6 as well as transitions in DyC_2 and Nd [64] and structural transitions in boracites, e.g., $Ni_3B_7O_{13}J$ [67] are described by $n = 6$. Transitions in MnSe, NiO, and ErSb [64] as well as in some other materials [68] are described by $n = 8$. Phase transitions in solids described by $n = 12$ order parameters are also known [68].

This list is far from being exhaustive. It enumerates order parameters describing the bulk phase transitions. An analogous picture should be expected in the case of the crack-tip transformational process zones. It should be further expected that a zone controlled by a multicomponent order parameter may exhibit different phases under different dynamic and/or external thermodynamic conditions, contain several phases at once, and as a result demonstrate a complex dynamic behavior.

In this paper, we address the general case of a process zone parametrized by an n-component order parameter. We

describe a concerted propagation of the crack-tip–process zone complex. It is described by a system of generalized time-dependent Ginzburg-Landau–type equations supplemented by mechanical ones. We explicitly eliminate the variable describing the transformation-generated strain, and reduce the problem to a system of integrodifferential equations solely in terms of the order parameter. We, further, argue that this system exhibits a bifurcation corresponding to the emergence of a process zone.

Applying the techniques of bifurcation theory, we show that the difference $\Delta T_* = T_* - T_c$ between the temperature of the emergence of the zone T_* and the transition temperature T_c universally scales with the stress intensity factor K_I, as $\Delta T_* \sim K_I^{4/3}$, and that at a high speed V of the crack-process zone complex, the zone universally vanishes upon achieving a critical velocity $V_* \sim K_I^{2/3}$. We further reduce the integrodifferential system to an algebraic system of ramification equations, enabling one to analyze its solutions and build a dynamic phase diagram in the stress intensity factor-temperature plane (K_I, T) in which the region of the zone's existence is determined. We, finally, make numerical estimates showing that the region of the zone's existence occupies a considerable part of the dynamic phase diagram.

II. BULK PHASE TRANSITIONS AS THE BASIS OF THE PROCESS ZONE DESCRIPTION

A. Order parameter

The very notion of "process zone" implies that a small domain in the immediate vicinity of the tip of a brittle crack has specific properties, different from those in the bulk. Only in such a case can the process zone be distinguished from the rest of the solid. This may be an abrupt *quantitative* variation of physical properties, such as a steep growth of the elastic nonlinearity [69] or a hyperelasticity [70] at the tip.

Alternatively, the process zone may exhibit a *qualitative* difference from the bulk, such as a difference in chemical composition, in crystal structure (e.g., cubic, tetragonal, or monoclinic lattice structures), in electronic structure (e.g., metal or isolator, exciton condensate or exciton gas, normal or superconductive, etc.), or in magnetic structure (paramagnetic, ferromagnetic, antiferromagnetic, or helicoid, etc.). All the above structures are related to certain internal degrees of freedom activated locally in the vicinity of the crack tip due to a high tensile and/or shear stress.

All such internal degrees of freedom can be divided into two classes: (i) the ones characterized by a potential, such as the Landau potential, playing the role of a Lyapunov function for their dynamics and (ii) those whose dynamics cannot be related to any potential. The structural degrees of freedom, such as optical and acoustic phonons, magnons, degrees of freedom related to an electronic subsystem, belong to the first class, while the degrees of freedom describing chemical reactions belong to the second one. The analysis of equations describing systems belonging to these two classes requires different approaches. In this paper, we only focus on the first class.

A set of degrees of freedom of the solid responsible for the qualitative difference between the zone and the bulk of the solid can always be extracted from the microscopic degrees of freedom, such as the normal coordinates of optical phonons, etc. They are referred to as the *order parameter* $\boldsymbol{\eta}$. We parametrize the differences in the solid properties inside the zone from those outside by a field $\boldsymbol{\eta} = \boldsymbol{\eta}(\mathbf{r},t)$. Without loss of generality, one may assume $\boldsymbol{\eta} \neq 0$ inside the zone, while vanishing outside. In this respect, our approach is akin to the theory of phase transitions [35] as well as to the popular phase field approach [71]. In contrast to the latter, however, our order parameter explicitly describes the degrees of freedom within the process zone responsible for the variation of its crystal, magnetic, or electronic structure.

With respect to the formation of the process zone, all order parameters of the first class can be divided into two subclasses. The order parameters belonging to the first subclass transform according to the same irreducible representation as the strain tensor $\boldsymbol{\varepsilon} = \boldsymbol{\varepsilon}(\mathbf{r})$ or some of its component(s) under the action of elements of the symmetry group of the solid crystal lattice. These are referred to as the *proper ferroelastic* phase transitions. The equation for the order parameter admits in this case an absolute term $\sim\boldsymbol{\varepsilon}$, and the process zone exists at all values of the temperature and stress intensity. Far from the tip, such an order parameter has the asymptotics $\boldsymbol{\eta} \sim \boldsymbol{\varepsilon}(\mathbf{r})$. The crystal structure of such a zone can be obtained by superimposing the strain corresponding to the order parameter onto the crystal lattice of the bulk phase.

The number of materials belonging to the second subclass by far exceeds that of the first one. In this subclass, the order parameter and the strain tensor components transform according to different irreducible representations of the symmetry group. Therefore, the strain has an *indirect* effect on the onset of the order parameter. For this reason, the process zone only emerges as soon as a certain thermodynamic condition is met: a critical temperature, or a critical value of the stress intensity factor, should be exceeded. In contrast to the first subclass, in this second subclass the process zone exhibits the features of a bifurcation.

The above classification can be applied if a group-subgroup relation exists between the symmetry of the phases taking place in the process zone. An additional possibility for applying this classification is the case that the process zone and the matrix symmetries are subgroups of a common symmetry group. Transitions referred to as "reconstructive" (including an important family of martensitic transformations) exhibit no such relations, and require a special modification of the Landau theory [65,72].

We focus here on the zones of the second subclass of the first class, while the ferroelastic, reconstructive, and martensitic transitions are outside the scope of this paper.

B. Invariants

The basis $\boldsymbol{\eta} = (\eta^1, \eta^2, \ldots, \eta^n)$ of the irreducible representations $\mathfrak{R}^n$ is normalized such that the symmetry operations of the group $\mathfrak{G}$ transform any n-dimensional sphere in the Euclidean space E^n into itself. Accordingly, one finds that the expression

$$J_2 = \sum_{i=1}^{n} (\eta^i)^2 \tag{1}$$

always represents an invariant with respect to $\mathfrak{G}$. In this paper the Latin superscripts are reserved to indicate components of the order parameter. To avoid confusion between superscripts and powers, we wrap the superscripted variables by round brackets, if necessary. Thus, η^2 means the second η component, while $(\eta^2)^2$ means this component squared.

There can be a few other rational invariants that are algebraically independent from one another. Together they form the so-called *integer rational basis of invariants* [43]. The existence of an invariant of the basis, different from J_2, as well as its possible structure, is not universal, but depends on the group $\mathfrak{G}$. We here build our further argumentation assuming the most general form of these invariants. This general form is formulated below.

In some (rather rare) cases, the symmetry group $\mathfrak{G}$ admits a cubic invariant. Its most general form can be written as follows:

$$J_3 = \sum_{i,j,k=1}^{n} \gamma_3^{ijk} \eta^i \eta^j \eta^k, \tag{2}$$

where the factors γ_3^{ijk} take integer values, such as 0, 1, 2, etc., providing the necessary structure of the invariant.

To give an example, let us consider the two-dimensional (2D) vector representation of the group $\mathfrak{G} = C_{3V} = 3m$. The first group name, C_{3V}, is given according to the Schoenflies, and the second, $3m$, to the International notation. The corresponding irreducible representation is indicated by E (see, e.g., [73]). One finds $\gamma_3^{111} = 1$, $\gamma_3^{112} = -3$, while all other components of the tensor $\boldsymbol{\gamma}_3$ are equal to zero. This yields $J_3 = (\eta^1)^3 - 3(\eta^1)^2\eta^2$. As another example, for the 3D representation T_2 of the group $\mathfrak{G} = T_d = \bar{4}3m$ [73], one finds all components γ_3^{ijk} equal to zero except $\gamma_3^{123} = 1$, yielding $J_3 = \eta^1\eta^2\eta^3$.

The general forms of the invariants of the fourth, fifth, and sixth orders belonging to the integer rational basis can be written analogously:

$$J_4(s) = \sum_{i,j,k,l=1}^{n} \gamma_4^{ijkl}(s) \eta^i \eta^j \eta^k \eta^l, \tag{3}$$

$$J_5(s) = \sum_{i,j,k,l,u=1}^{n} \gamma_5^{ijkl}(s) \eta^i \eta^j \eta^k \eta^l \eta^u, \tag{4}$$

and

$$J_6(s) = \sum_{i,j,k,l,u,v=1}^{n} \gamma_6^{ijkluv}(s) \eta^i \eta^j \eta^k \eta^l \eta^u \eta^v, \tag{5}$$

where the tensors $\boldsymbol{\gamma}_4$, $\boldsymbol{\gamma}_5$, and $\boldsymbol{\gamma}_6$ play the same roles as that of the tensor $\boldsymbol{\gamma}_3$ and $s = 1,2,\ldots,m_p$, where $p = 4$, 5, or 6 enumerate the independent fourth, fifth, and sixth order invariants, if any of them are allowed by the group $\mathfrak{G}$. In fact, their number m_p can only in some rare cases be greater than 1. They are completely determined by the representation $\mathfrak{R}^n$. As in the previous case, if there are no invariants of order 4, 5, or 6, all the components of the corresponding tensor $\boldsymbol{\gamma}_4$, $\boldsymbol{\gamma}_5$, or $\boldsymbol{\gamma}_6$ are equal to zero. For example, in the case of the group $\mathfrak{G} = T_d$ one finds a single independent invariant of the fourth order $m_4 = 1$ and all $\gamma_4^{ijkl}(1) = 0$ except $\gamma_4^{1111}(1) = \gamma_4^{2222}(1) = \gamma_4^{3333}(1) = 1$, giving $J_4 = (\eta^1)^4 + (\eta^2)^4 + (\eta^3)^4$.

One should keep in mind that the relations (2)–(5) only describe independent invariants. These are the invariants that cannot be obtained from the ones of the lower order by applying algebraic operations: addition, subtraction, multiplication, and raising to any integer power. Not to account for them twice, the factors $\gamma_n^{ijkl}(s)$ with $n = 3$, 4, 5, and 6 corresponding to the dependent invariants in (3), (4), and (5) are assumed to be equal to zero.

Further, the group $\mathfrak{G}$ only allows a few independent invariants. Thus, some (or all) of the invariants (2)–(5) may appear to be forbidden by the symmetry. For example, in the case of the group $\mathfrak{G} = C_{3V}$, the only independent invariants are of the second and the third order, while for $\mathfrak{G} = T_d$, there are only second-, third-, and fourth-order independent invariants. Correspondingly, in the $\mathfrak{G} = C_{3V}$ case, one has to choose all components $\boldsymbol{\gamma}_4 = \boldsymbol{\gamma}_5 = \boldsymbol{\gamma}_6 = 0$, while in the case of the group $\mathfrak{G} = T_d$ one finds $\boldsymbol{\gamma}_5 = \boldsymbol{\gamma}_6 = 0$.

C. Landau potential

The invariants discussed in the previous section enable one to build the nonequilibrium Landau potential (also referred to as the *Landau potential*) describing the phase transition in the bulk of the crystal. Since the Landau potential must be invariant with respect to all transformations of the group $\mathfrak{G}$, it represents the expansion in terms of the above invariants as well as of the strain tensor components:

$$\Phi_{\text{bulk}}(\boldsymbol{\eta},\boldsymbol{\varepsilon}) = \Phi_{\text{pt}}(\boldsymbol{\eta}) + \Phi_{\text{el}}(\boldsymbol{\varepsilon}) + \Phi_{\text{int}}(\boldsymbol{\eta},\boldsymbol{\varepsilon}), \tag{6}$$

where $\boldsymbol{\varepsilon} \equiv \varepsilon_{\alpha\beta}$ is the strain tensor

$$\varepsilon_{\alpha\beta} = \frac{1}{2}\left(\frac{\partial u_\alpha}{\partial x_\beta} + \frac{\partial u_\beta}{\partial x_\alpha}\right),$$

u_α being the displacement vector. The Greek subscripts α, $\beta, \ldots = 1,2,3$ enumerate the tensor indices in the three-dimensional (3D) Euclidean space E^3, and the Einstein summation convention over the Greek indices is adopted.

Further, the function $\Phi_{\text{pt}}(\boldsymbol{\eta})$ denotes a part responsible for the phase transition:

$$\Phi_{\text{pt}}(\boldsymbol{\eta}) = \frac{a}{2}J_2 + \frac{b_3}{3}J_3 + \Phi_4 + \Phi_5 + \Phi_6 + \cdots, \tag{7}$$

where for the sake of brevity, we denote by Φ_4, Φ_5, and Φ_6 the contributions of the fourth, fifth, and sixth orders in terms of the order parameter:

$$\Phi_4 = \frac{b_4^{(0)}}{4}J_2^2 + \frac{1}{4}\sum_{s=1}^{m_4} b_4(s)J_4(s), \tag{8}$$

$$\Phi_5 = \frac{b_5^{(0)}}{5}J_2J_3 + \frac{1}{5}\sum_{s=1}^{m_5} b_5(s)J_5(s), \tag{9}$$

$$\Phi_6 = \frac{b_6^{(0)}}{6}J_2^3 + \frac{b_6^{(1)}}{6}J_3^2 + \frac{b_6^{(2)}}{6}J_2J_4 + \frac{1}{6}\sum_{s=1}^{m_6} b_6(s)J_6(s). \tag{10}$$

The former terms in (8)–(10) represent combinations of the invariants belonging to the integer rational basis.

We adopt the classical assumption of the Landau theory [35,43,44], that $a = a_0(T - T_c)$, where T is the temper-

ature, T_c is the Curie temperature, and $a_0 > 0$ and $b_k^{(l)}$ (with $k = 3, 4, 5$, and 6 and $l = 0,1,2\ldots$) are constants.

It should be noted that the expression (7) represents the Taylor expansion of the Landau potential density in terms of the components of the order parameter. The minimum requirement for the truncation of this series is that the higher order terms must be positive defined at $\eta \to \infty$. Thus, if Φ_4 is positive defined, the expansion can be limited to the fourth order terms, while Φ_5, if any, and Φ_6 can be disregarded. In this case, the bulk phase transition appears to be of the second order if $b_3 \equiv 0$, or of the first order everywhere except an isolated Curie point otherwise [35].

If Φ_4 is not positive definite, one needs to retain the higher order terms, and if Φ_6 is positive definite, the series can be truncated here. The bulk phase transition in this case is of the first order everywhere. Further, a complete description of the phase diagram may require expanding the Landau potential density up to still higher order terms. We do not go here into a discussion of these details, but refer the reader to the book [43]. The extension of the theory to account for higher order terms is straightforward, but in a general form it is cumbersome. $\Phi_{el}(\varepsilon_{\alpha\beta})$ is the elastic part of the Landau potential density:

$$\Phi_{el}(\boldsymbol{\varepsilon}) = \tfrac{1}{2} C_{\alpha\beta\gamma\delta}\varepsilon_{\alpha\beta}\varepsilon_{\gamma\delta}, \tag{11}$$

where $\mathbf{C} \equiv C_{\alpha\beta\gamma\delta}$ is the tensor of elastic moduli.

Finally, $\Phi_{int}(\boldsymbol{\eta},\boldsymbol{\varepsilon})$ is the term describing the interaction between the strain and the order parameter. Within the Landau approach, one usually assumes the interaction energy is linear in the strain and quadratic in the order parameter [74]. In the most general form, it can be written as follows:

$$\Phi_{int}(\boldsymbol{\eta},\boldsymbol{\varepsilon}) = \sum_{i,j=1}^{n} A_{\alpha\beta}^{ij}\varepsilon_{\alpha\beta}\eta^i\eta^j, \tag{12}$$

where $A_{\alpha\beta}^{ij}$ is the tensor of striction constants in the space $E^3 \otimes E^n$. Any solid symmetry group $\mathfrak{G}$ allows the existence of the dilatant interaction term (12) $\varepsilon_{\alpha\alpha}\sum_{i=1}^{n}(\eta^i)^2$ corresponding to the diagonal tensor of the striction constants $A_{\alpha\beta}^{ij} \sim \delta^{ij}\delta_{\alpha\beta}$, where $\delta_{\alpha\beta}$ and δ^{ij} are the Kronecker deltas. However, some crystal symmetries admit nondeviatoric contributions as well. In this case, the tensor of striction constants $A_{\alpha\beta}^{ij}$ possesses off-diagonal terms.

D. Elimination of the elastic variables in the homogeneous case

The stress tensor is expressed as $\sigma_{\alpha\beta} = \partial\Phi/\partial\varepsilon_{\alpha\beta}$, yielding

$$\sigma_{\alpha\beta} = C_{\alpha\beta\gamma\delta}\varepsilon_{\gamma\delta} + \sum_{i,j=1}^{n} A_{\alpha\beta}^{ij}\eta^i\eta^j. \tag{13}$$

The last term in (13) describes the spontaneous stress generated by the phase transition. In the homogeneous, stress-free state ($\sigma_{\alpha\beta} = 0$), one finds

$$\varepsilon_{\alpha\beta} = -\sum_{i,j=1}^{n} Q_{ab}^{ij}\eta^i\eta^j, \tag{14}$$

where $Q_{\alpha\beta}^{ij}$ can also be referred to as the striction tensor, and the tensors $A_{\gamma\delta}^{ij}$ and $Q_{\alpha\beta}^{ij}$ are related to one another as follows:

$$Q_{\alpha\beta}^{ij} = S_{\alpha\beta\gamma\delta}A_{\gamma\delta}^{ij}; \quad A_{\alpha\beta}^{ij} = C_{\alpha\beta\gamma\delta}Q_{\gamma\delta}^{ij}. \tag{15}$$

Here, $\mathbf{S}$ is the compliance tensor: $\mathbf{S} = \mathbf{C}^{-1}$. The tensor $Q_{\alpha\beta}^{ij}$ may be convenient to use since in many cases the striction constants are available in this form (see, e.g., [59]). Substituting (14) into $\Phi_{el}(\boldsymbol{\varepsilon}) + \Phi_{int}(\boldsymbol{\eta},\boldsymbol{\varepsilon})$ [Eqs. (11) and (12)], one finds the fourth-order term in the form

$$\Phi_4' = \frac{1}{4}b_4^{(0)}J_2^2 + \frac{1}{4}\sum_{s=1}^{m_4} R_0^{ijkl}(s)\eta^i\eta^j\eta^k\eta^l, \tag{16}$$

where

$$R_0^{ijkl}(s) = b_4(s)\gamma_4^{ijkl}(s) - \frac{1}{2}S_{\alpha\beta\gamma\delta}A_{\alpha\beta}^{ij}A_{\gamma\delta}^{kl}. \tag{17}$$

The nonequilibrium Landau potential of the bulk phase transition takes the form

$$\Phi_{bulk}(\boldsymbol{\eta},\boldsymbol{\varepsilon}) = \frac{a}{2}J_2 + \frac{b_3}{3}J_3 + \Phi_4' + \Phi_5 + \Phi_6 + \cdots. \tag{18}$$

The Landau potential $\Phi_{bulk}(\boldsymbol{\eta},\boldsymbol{\varepsilon})$ [Eq. (18)] describes a solid with the same symmetry $\mathfrak{G}$ as that described by (6). This forces it to have the same structure as that exhibited by (8). Thus, the effect of the elimination of the elastic variables only renormalizes the coefficients $b_4^{(0)}$ and $b_4(s)$.

E. Classification of the phases

A solid is characterized by its crystallographic space group G acting in physical 3D space E_3. The order parameter represents a set of degrees of freedom or their linear combinations $\boldsymbol{\eta} = (\eta^1,\eta^2,\ldots,\eta^n)$ (such as the displacements of the atoms, magnetic moments, etc.) transforming according to the irreducible representations $\mathfrak{R}^n$ of the group G. The degrees of freedom belonging to the irreducible representation are transformed into one another by the group operations, but those belonging to different irreducible representations are independent of one another.

Each irreducible representation forms a point group $\mathfrak{G}$ of $n \times n$ matrices in the n-dimensional Euclidean space E^n spanned by $\boldsymbol{\eta}$, where n is a natural number $n = 1,2,\ldots$. The order parameter $\boldsymbol{\eta} = (\eta^1,\eta^2,\ldots,\eta^n)$ represents a vector in E^n. The state in which $\boldsymbol{\eta} = 0$ is invariant with respect to all transformations of the group $\mathfrak{G}$. It, thus, describes the mother phase.

The $\boldsymbol{\eta}$ vectors with at least some components different from zero (such as $\eta^1 \neq 0$; $\eta^2 = \eta^3 = \cdots = 0$, or $\eta^1 = \eta^2 \neq 0$; $\eta^3 = \cdots = 0$, etc.) describe possible "daughter" phases with different symmetry groups $\mathfrak{G}_1$, $\mathfrak{G}_2$, ...equal to the subgroups of the mother phase ($\mathfrak{G}_1 \subset \mathfrak{G}$, $\mathfrak{G}_2 \subset \mathfrak{G}, \ldots$) leaving the corresponding vector $\boldsymbol{\eta}$ invariant. They correspond to the space subgroups of the group G: $\mathfrak{G}_i \to G_i \subset G$. These relations classify the symmetries of all possible daughter phases.

The $\boldsymbol{\eta}$ vectors differing from one another only by the sign of some of the components, such as the pair $(\eta,0,0\ldots)$ and $(-\eta,0,0\ldots)$ or the pair $(\eta,\eta,0,\ldots)$ and $(\eta,-\eta,0,\ldots)$, exhibit the same symmetry group and correspond to the structures

referred to as "domains," "twins," or "variants" by different communities [75].

Up to this point a standard theory of phase transitions in a homogeneous solid has been briefly reviewed and reformulated in the form necessary to communicate our results. The description of the results will start in the next section.

III. EQUATIONS OF MOTION FOR THE ORDER PARAMETER

From now on, let us consider a solid with an inhomogeneity. It is introduced by a spatially inhomogeneous (and, eventually, time-dependent) strain field $\boldsymbol{\varepsilon}^{(0)}(\mathbf{r},t)$ in the bulk of the solid. It can have various origins, such as solid defects (cracks, dislocations, disclinations, grain walls, etc.) or either sound or shock waves. We do not specify its origin at the moment.

A. Density of the nonequilibrium Landau potential

In the inhomogeneous case, the order parameter depends on the coordinates and, eventually, on the time: $\boldsymbol{\eta} = \boldsymbol{\eta}(\mathbf{r},t)$. One finds

$$\Phi(\boldsymbol{\eta},\boldsymbol{\varepsilon}) = \Phi_{\rm g}(\boldsymbol{\eta}) + \Phi_{\rm pt}(\boldsymbol{\eta}) + \Phi_{\rm el}(\boldsymbol{\varepsilon}) + \Phi_{\rm int}(\boldsymbol{\eta},\boldsymbol{\varepsilon}). \tag{19}$$

The term $\Phi_{\rm g}$ in (7) has the form

$$\Phi_{\rm g} = \frac{g}{2}\sum_{i=1}^{n}(\nabla\eta^i)^2. \tag{20}$$

It accounts for the energy penalty for the order parameter's inhomogeneity. Here, $\nabla\eta^i$ is the gradient of the order parameter and $g > 0$ is a constant. It should be mentioned that the constants g, a_0, $b_n(s)$, $T_{\rm c}$, and $A^{ij}_{\alpha\beta}$ (or $Q^{ij}_{\alpha\beta}$) describing the phase transformation together with the tensor of elastic moduli $\mathbf{C}$ represent *material constants* of the solid.

B. Lagrangian and the dissipation function

Making use of the density of the Landau potential (19), one can write a Lagrangian $\mathfrak{L}$ and a dissipation function $\mathfrak{D}$ of the solid:

$$\mathfrak{L} = \int\left\{\frac{1}{2}\rho\left(\frac{\partial u_\alpha}{\partial t}\right)^2 - \Phi(\boldsymbol{\eta},\boldsymbol{\varepsilon})\right\}d\Omega, \tag{21}$$

$$\mathfrak{D} = \frac{\kappa}{2}\int\sum_{i=1}^{n}\left(\frac{\partial\eta^i}{\partial t}\right)^2 d\Omega, \tag{22}$$

where ρ is the mass density of the solid, Φ is the density of the Landau potential, t is the time, κ is the kinetic constant of the order parameter, and Ω denotes the spatial domain. Since here we only consider the case of a thin plate, Ω represents the infinite plane and $d\Omega \equiv dx\,dy$. We, thus, assign both $\mathfrak{L}$ and $\mathfrak{D}$ to the unit solid thickness in the z direction.

It should be stressed that we only consider a brittle solid. Therefore, the dissipation function contains no plasticity-generated terms and only describes the dissipation due to the dynamics of the order parameter.

C. Equations of motion

The equations of motion (the dynamic Ginzburg-Landau equations) for the order parameter together with the mechanical equations can be derived by the variation of the action $S = \int\mathfrak{L}\,dt$ using the Lagrangian (21) and the dissipation function (22), the variation of the action with respect to each generalized coordinate being equated to the variation of the dissipation function with respect to the corresponding generalized velocity:

$$\frac{\delta\mathfrak{D}}{\delta(\partial\eta^i/\partial t)} = \frac{\delta\mathfrak{L}}{\delta\eta^i} \tag{23}$$

as is described in [76], where δ indicates the variational derivative. Equation (23) represents the Onsager equations for the order parameters. One finds

$$\kappa\frac{\partial\eta^i}{\partial t} = g\Delta\eta^i - a\eta^i - \sum_{j=1}^{n}A^{ij}_{\alpha\beta}\varepsilon_{\alpha\beta}\eta^j - N^i(\boldsymbol{\eta}), \tag{24}$$

where Δ is the Laplace operator and $N^i(\boldsymbol{\eta})$ is the nonlinear term of the ith equation. Namely, it consists of the terms of the third, fourth, fifth, and sixth orders in $\boldsymbol{\eta}$:

$$\mathbf{N}(\boldsymbol{\eta}) = \mathbf{N}_3(\boldsymbol{\eta}) + \mathbf{N}_4(\boldsymbol{\eta}) + \mathbf{N}_5(\boldsymbol{\eta}) + \mathbf{N}_6(\boldsymbol{\eta}),$$

where

$$N^i_3(\boldsymbol{\eta}) = \sum_{j,k=1}^{n}b_3\gamma_3^{ijk}\eta^j\eta^k, \tag{25}$$

$$N^i_4(\boldsymbol{\eta}) = b_4^{(0)}\eta^i\sum_{j=1}^{n}(\eta^j)^2 + \sum_{s=1}^{m_4}\sum_{j,k,l=1}^{n}b_4(s)\gamma_4^{ijkl}(s)\eta^j\eta^k\eta^l, \tag{26}$$

$$N^i_5(\boldsymbol{\eta}) = \frac{b_5^{(0)}}{5}\left(2\eta^i J_3 + 3J_2\sum_{j,k=1}^{n}\gamma_3^{ijk}\eta^j\eta^k\right) + \sum_{s=1}^{m_5}\sum_{j,k,l,u=1}^{n}b_5(s)\gamma_5^{ijklu}(s)\eta^j\eta^k\eta^l\eta^u, \tag{27}$$

and $N^i_6(\boldsymbol{\eta})$, which for the sake of readability we divided into three items: $N^i_6(\eta) = N^i_{6A} + N^i_{6B} + N^i_{6C}$, where

$$N^i_{6A} = b_6^{(0)}\eta^i J_2^2 + \frac{b_6^{(1)}}{2}J_3\sum_{j,k=1}^{n}\gamma_3^{ijk}\eta^j\eta^k, \tag{28}$$

$$N^i_{6B} = \frac{b_6^{(2)}}{6}\left[2\eta^i J_4 + 4J_2\sum_{s=1}^{m_4}\sum_{j,k,l=1}^{n}\gamma_4^{ijkl}(s)\eta^j\eta^k\eta^l\right], \tag{29}$$

and

$$N^i_{6c} = \sum_{s=1}^{m_6}\sum_{j,k,l,u,v=1}^{n}b_6(s)\gamma_6^{ijkluv}(s)\eta^j\eta^k\eta^l\eta^u\eta^v. \tag{30}$$

We would like to stress that this highly complex form of the nonlinear part of the order parameter equations originates from keeping the approach general. In specific cases, most of the invariants are forbidden by the symmetry. This never removes a nonlinear part completely, but makes it more concise.

The mechanical equations of motion can be obtained by setting equal to zero the variation of the action functional with respect to the components of the displacement vector u_α as follows: $\delta\mathfrak{L}/\delta u_\alpha = 0$. They have the standard form

$$\rho\frac{\partial^2 u_\alpha}{\partial t^2} = \frac{\partial \sigma_{\alpha\beta}}{\partial x_\beta}, \tag{31}$$

where, however, the stress tensor accounts for the phase transformation according to the relation (13). Equations (24) and (31) represent a system of $n+3$ equations completely describing the concerted dynamics of the order parameter and acoustics caused by the inhomogeneous, time-dependent strain field.

D. Elimination of the elastic variables

Making use of Eqs. (24), (31), and (13), one can express the displacement vector u_α as

$$u_\alpha(\mathbf{r},t) = u_\alpha^{(0)}(\mathbf{r},t) - \sum_{i,j=1}^{n} A_{\delta\gamma}^{ij}\int G_{\alpha\delta}(\mathbf{r}-\mathbf{r}',t-t') \times \frac{\partial[\eta^i(\mathbf{r}',t')\eta^j(\mathbf{r}',t')]}{\partial x_\gamma'} d^2r'dt', \tag{32}$$

where $u_\alpha^{(0)}(\mathbf{r},t)$ $(\alpha = 1,2,3)$ are the displacements in the solid in the absence of the order parameter field. These displacements represent solutions for $u_\alpha^{(0)}(\mathbf{r},t)$ obtained within the approach of the classical mechanics. These solutions are assumed to be known. Further, $G_{\alpha\beta}(\mathbf{r},t)$ is the elastic Green's function of the solid with a cut and no zone. This means that it is taken at $\eta \equiv 0$. This enables one to find the Fourier transform of the displacement field $u_\alpha(\mathbf{k},\omega)$:

$$u_\alpha(\mathbf{k},\omega) = u_\alpha^{(0)}(\mathbf{k},\omega) - iG_{\alpha\gamma}(\mathbf{k},\omega)k_\beta\sum_{i,j=1}^{n} A_{\gamma\beta}^{ij}\Theta^{ij}(\mathbf{k},\omega), \tag{33}$$

where $u_\alpha^{(0)}(\mathbf{k},\omega)$ is the Fourier transform of $u_\alpha^{(0)}(\mathbf{r},t)$, while $\Theta^{ij}(\mathbf{k},\omega)$ is expressed as follows:

$$\Theta^{ij}(\mathbf{k},\omega) = \int \eta^i(\mathbf{r},t)\eta^j(\mathbf{r},t)\exp[i(\omega t - \mathbf{k}\cdot\mathbf{r})]d\Omega\, dt \tag{34}$$

and $G_{\alpha\beta}(\mathbf{k},\omega) = \int G_{\alpha\beta}(\mathbf{r},t)\exp[i(\omega t - \mathbf{k}\cdot\mathbf{r})]d\Omega\, dt$ is the Fourier transform of the elastic Green's function. One should not confuse here the imaginary unit in the Fourier transform with the index i of the order parameter η^i. To the best of our knowledge, the elastic Green's function of a plane with a cut is unknown. We approximate it by the elastic Green's function of the intact elastic plane

$$G_{\alpha\gamma}(\mathbf{k},\omega) = \|C_{\alpha\beta\gamma\delta}k_\beta k_\delta - \rho\omega^2\delta_{\alpha\gamma}\|^{-1} \tag{35}$$

expressed in terms of the tensor of the elastic moduli. This enables one to express the strain $\varepsilon_{\alpha\beta}(\mathbf{k})$ in the form

$$\varepsilon_{\alpha\beta}(\mathbf{k},\omega) = \varepsilon_{\alpha\beta}^{(0)}(\mathbf{k},\omega) - \frac{1}{2}k_\gamma[k_\beta G_{\alpha\delta}(\mathbf{k},\omega) + k_\alpha G_{\beta\delta}(\mathbf{k},\omega)] \times \sum_{i,j=1}^{n} A_{\delta\gamma}^{ij}\Theta^{ij}(\mathbf{k},\omega), \tag{36}$$

where $\varepsilon_{\alpha\beta}^{(0)}(\mathbf{k},\omega)$ is the Fourier transform of the strain, $\varepsilon_{\alpha\beta}^{(0)}(\mathbf{r},t) = [\partial u_\alpha^{(0)}(\mathbf{r},t)/\partial x_\beta + \partial u_\beta^{(0)}(\mathbf{r},t)/\partial x_\alpha]/2$, generated at $\eta \equiv 0$. The second term (36) represents the contribution of the order parameter to the strain field in the solid.

Passing from k to x space and substituting the strain expression (36) into (24), one explicitly eliminates the strain generated by the phase transformation, and obtains a system of n nonlinear, integrodifferential equations of motion for the order parameter:

$$\kappa\frac{\partial\eta^i}{\partial t} = g\Delta\eta^i - a\eta^i - \sum_{j=1}^{n} A_{\alpha\beta}^{ij}\varepsilon_{\alpha\beta}^{(0)}(\mathbf{r},t)\eta^j - N^i(\boldsymbol{\eta}) - \Delta N^i(\boldsymbol{\eta}). \tag{37}$$

Here,

$$\Delta N^i(\boldsymbol{\eta}) = -\sum_{j,l,m=1}^{n}\eta^j(\mathbf{r},t)\int K^{ijlm}(\mathbf{k},\omega)\Theta^{lm}(\mathbf{k},\omega) \times \exp[i(\mathbf{k}\cdot\mathbf{r} - \omega t)]\frac{d^2k\, d\omega}{(2\pi)^3}, \tag{38}$$

where the kernel $K^{ijlm}(\mathbf{k})$ takes the form

$$K^{ijlm}(\mathbf{k},\omega) = A_{\alpha\beta}^{ij}A_{\gamma\delta}^{lm}k_\gamma k_\beta G_{\alpha\delta}(\mathbf{k},\omega). \tag{39}$$

Let us observe that since $\Theta^{lm}(\mathbf{k},\omega) \sim \eta^2$ [Eq. (34)], the contribution $\Delta N^i(\boldsymbol{\eta})$ is cubic in terms of the order parameter $\boldsymbol{\eta}$.

The integrodifferential system (37) consists of n equations. It describes the dynamics of the inhomogeneous distribution of the n-component order parameter $\boldsymbol{\eta}$ engendered by the dynamics of an elastic inhomogeneity. The latter is implemented by $\varepsilon_{\alpha\beta}^{(0)}(\mathbf{r},t)$, describing the strain of the solid with no order parameter field.

Since the strain of the bare system $\varepsilon_{\alpha\beta}^{(0)}(\mathbf{r},t)$ is known, at least in principle, one finds that the bare solid stress $\sigma_{\alpha\beta}^{(0)}(\mathbf{r},t) = C_{\alpha\beta\gamma\delta}\varepsilon_{\alpha\beta}^{(0)}(\mathbf{r},t)$ is also known. The use of the striction tensor $Q_{\alpha\beta}^{ij}$ instead of $A_{\alpha\beta}^{ij}$ enables one to rewrite (37) in a more concise form:

$$\kappa\frac{\partial\eta^i}{\partial t} = g\Delta\eta^i - a\eta^i - \sum_{j=1}^{n} Q_{\alpha\beta}^{ij}\sigma_{\alpha\beta}^{(0)}(\mathbf{r},t)\eta^j - N^i(\boldsymbol{\eta}) - \Delta N^i(\boldsymbol{\eta}). \tag{40}$$

Up to this point of the paper, the origin of the field $\varepsilon_{\alpha\beta}^{(0)}(\mathbf{r},t)$ has not been specified. It may be caused by any stress concentrator: the crack tip, a dislocation, or their array, a twin or grain boundary, inclusion, etc. Alternatively, it may be caused by a sound or a propagating shock wave.

Equations (37) valid for the second subclass of the first class of materials have been derived without any limitations. They describe, therefore, the formation of transformational zones in the vicinity of elastic inhomogeneities of any origin, both in statics and dynamics. Moreover, (37) is capable of describing a soft (second-order-like) zone emergence as well as the hard (first-order-like) one.

E. Specifying the crack-tip process zone

From now on, we narrow our considerations to a process zone at a crack tip by specifying a tip-generated elastic stress

$$\sigma^{(0)}_{\alpha\beta}(\mathbf{r},t) = \frac{K_I}{(2\pi r)^{1/2}}\varphi_{\alpha\beta}(\theta), \tag{41}$$

where K_I is the stress intensity factor, and r and θ are polar coordinates with origin at the crack tip.

F. Automodel regime

In the following, we analyze a steady, rectilinear crack propagation with velocity $\mathbf{V}$. It is described by the automodel solution of the system of dynamic equations (37). Assuming $\boldsymbol{\eta} = \boldsymbol{\eta}(\mathbf{r} - \mathbf{V}t)$, and passing to the comoving frame $\mathbf{r}' = \mathbf{r} - \mathbf{V}t$, the system of equations of motion for $\boldsymbol{\eta} = \boldsymbol{\eta}(\mathbf{r}')$ [Eq. (37)] takes the form

$$\widehat{L}(a)\eta^i = N^i(\boldsymbol{\eta}) + \Delta N^i(\boldsymbol{\eta}), \tag{42}$$

where $\Delta N^i(\boldsymbol{\eta})$ has the form

$$\Delta N^i(\boldsymbol{\eta}) = -\sum_{j,l,m=1}^{n} \eta^j(\mathbf{r}') \int K^{ijlm}(\mathbf{k},\mathbf{k}\cdot\mathbf{V})\Theta^{lm}(\mathbf{k}) \times \exp(i\mathbf{k}\cdot\mathbf{r}')\frac{d^2k}{(2\pi)^3} \tag{43}$$

and in contrast to (38), depends on t only through $\mathbf{r}'$. In addition, the scalar product $\mathbf{k}\cdot\mathbf{V}$ is substituted instead of ω into $K^{ijlm}(\mathbf{k},\omega)$, while $\Theta^{lm}(\mathbf{k})$ is now defined as follows:

$$\Theta^{lm}(\mathbf{k}) = \int \eta^l(\mathbf{r}')\eta^m(\mathbf{r}')\exp(-i\mathbf{k}\cdot\mathbf{r}')d^2r'. \tag{44}$$

We, further, direct the x' axis along the direction of the crack propagation. The linear operator $\widehat{L}(a)$ in the left-hand part of Eq. (42) has the form

$$\widehat{L}(a)\eta^i = g\Delta'\eta^i + \kappa V\frac{\partial\eta^i}{\partial x'} - a\eta^i - \frac{K_I Q}{(2\pi r')^{1/2}}\sum_{j=1}^{n} B^{ij}(\theta)\eta^j \tag{45}$$

and we used the (40) form of the dynamic system. Here, Q is the norm and $B^{ij}(\theta)$ is the tensor of dimensionless striction constants:

$$Q = \sqrt{\sum\nolimits_{i,j=1}^{n}(Q^{ij}_{\alpha\beta})^2}, \tag{46}$$

$$B^{ij}(\theta) = \frac{Q^{ij}_{\alpha\beta}\varphi_{\alpha\beta}(\theta)}{Q}. \tag{47}$$

The Laplace operator Δ' in (45) is defined by $\Delta' = \partial^2/x'^2 + \partial^2/y'^2$ and $r' = (x'^2 + y'^2)^{1/2}$. Since in the following we only use the comoving frame, from here on the primes on x, y, r, and Δ are omitted.

To complete the statement of the mathematical problem one needs in addition to specify boundary conditions. If one describes a process zone $\eta^i(\mathbf{r}) \neq 0$ localized at the crack tip $(x,y) = 0$, and embedded in the matrix of the bulk phase ($\alpha > 0$, $\eta^i = 0$ for any i), the boundary condition takes the form

$$\eta^i(\infty) = 0 \quad (i = 1,2,\ldots,n). \tag{48}$$

Because the variation of atomic displacements must be limited, the order parameter is everywhere finite: $|\boldsymbol{\eta}| < \infty$. The same holds in the case of a magnetic, superconductive, and other order parameters unrelated to the atomic displacements.

Equation (42) describes the crack propagating steadily and rectilinearly, carrying the transformational process zone at its tip. It is highly nonlinear. Its complete study cannot be performed analytically, but it is numerically tractable. Let us observe, however, that Eq. (42) admits the exact trivial solution $\boldsymbol{\eta} \equiv 0$ describing the crack tip with no zone. For this reason, the problem of the emergence of the process zone can be formulated as that of a bifurcation of the trivial solution of Eq. (42). This results in the emergence of nontrivial solutions $\boldsymbol{\eta}(\mathbf{r}) \neq 0$, the problem admitting an analytical approach. This analytical solution is presented in the next section.

IV. BIFURCATION OF THE PROPAGATION EQUATION OF THE PROCESS ZONE

A. Bifurcation point

To analyze the emergence of a process zone at the tip of a crack propagating along the x axis with velocity $\mathbf{V} = (V,0)$, we apply bifurcation theory [77] to the system of equations (42). This theory is, however, only valid for soft (supercritical) bifurcations. This case takes place if the fourth-order terms in the nonequilibrium free energy density (8) are positive definite. This is assumed hereafter in this paper. Further, in general, the system may exhibit a whole cascade of bifurcations, but here we only focus on the first one. To find this one, it is enough to keep the Landau potential expansion up to the fourth order, while omitting the higher order terms.

The trivial solution $\boldsymbol{\eta} \equiv 0$ of (42) is stable at large values of a. It becomes, however, unstable below a certain a_*, and a solution with $\boldsymbol{\eta}(\mathbf{r}) \neq 0$ branches off from the trivial one. The bifurcation point a_* is the first discrete eigenvalue $a_* \equiv a_1$ of the linear operator $\widehat{L}$:

$$\begin{cases} \widehat{L}(a_p)\Psi^i_p(\mathbf{r}) = 0, \\ \Psi^i_p(\infty) = 0, \end{cases} \tag{49}$$

where a_p are the eigenvalues and the vector-valued function $\boldsymbol{\Psi}_p(\mathbf{r}) = (\Psi^1_p, \Psi^2_p, \ldots, \Psi^n_p)$ represents the set of the eigenfunctions of the operator $\widehat{L}(a)$ with p enumerating the discrete spectrum states: $p = 1,2,3\ldots$, while i specifies the component projection in the space E^n [77].

Our approach is essentially based on the following statement of bifurcation theory: the main term of the solution branching off from the trivial one always has the form

$$\eta^i(\mathbf{r}) = \xi^i\Psi^i_*(\mathbf{r}) + O(\xi^3), \tag{50}$$

where the amplitudes $\boldsymbol{\xi} = (\xi^1,\xi^2,\ldots,\xi^n)$ are to be determined later on [77]. Rescaling Eq. (49), $\boldsymbol{\rho} = \mathbf{r}/R$, where

$$R = \left[\frac{g}{QK_I\sqrt{2\pi}}\right]^{2/3} \tag{51}$$

is the characteristic process zone size, and looking for the eigenfunction $\Psi^i_*(\mathbf{r})$ in the following form:

$$\Psi^i_p(\boldsymbol{\rho}) = \exp\left(-\frac{\kappa VR}{2g}\rho\cos\theta\right) \times \psi^i_p(\boldsymbol{\rho}) \tag{52}$$

one passes to the eigenvalue equation on ψ_p^i:

$$\begin{cases} \widetilde{\Delta}\psi_p^i - \sum_{j=1}^{n} U^{ij}(\rho,\theta)\psi_p^j(\boldsymbol{\rho}) = \lambda_p \psi_p^i, \\ \psi_p^i(\infty) = 0, \end{cases} \tag{53}$$

where the Laplace operator $\widetilde{\Delta} = \partial^2/\partial\rho^2 + \rho^{-1}\partial/\partial\rho + \rho^{-2}\partial^2/\partial\theta^2$ is written in terms of the dimensionless coordinates ρ and θ.

It should be noted that (53) represents an n-component Schrödinger equation, the last terms in the left-hand part (53) playing the role of its potential:

$$U^{ij}(\rho,\theta) = \frac{1}{\sqrt{\rho}} B^{ij}(\theta). \tag{54}$$

The discrete eigenvalue a_p of Eq. (49) is related to the dimensionless eigenvalue λ_p ($p = 1,2,\ldots$) of the dimensionless Eq. (53) as follows:

$$a_* = \frac{\lambda_*}{g^{1/3}(2\pi)^{2/3}}(QK_I)^{4/3} - \frac{\kappa^2 V^2}{4g}. \tag{55}$$

One concludes that if (53) possesses a discrete spectrum with the ground state level $\lambda_1 = \lambda_*$, the a value corresponding to its ground state is $a_1 = a_*$, as described by (55).

From now on, let us assume that the discrete spectrum exists, and the ground state eigenvalue λ_* and the corresponding eigenfunctions $\boldsymbol{\psi}_*(\rho)$, along with $\boldsymbol{\Psi}_*(\rho)$, are known.

B. Ramification equations

To find the amplitude $\boldsymbol{\xi}$, one can substitute the solution (50) into the equation of the propagation of the zone (42) and rewrite the latter as follows:

$$\xi^i \exp\left(-\frac{\kappa V}{2g}x\right)\widehat{L}(\lambda_*)\psi_*^i = (a - a_*)\xi^i\Psi_*^i(\mathbf{r}) + N^i(\boldsymbol{\xi}\boldsymbol{\Psi}_*). \tag{56}$$

Here, $\Psi_*^i \equiv \Psi_1^i$ are the ground state eigenfunctions of Eq. (49). The linear operator $\widehat{L}$ [Eq. (53)] in the left-hand part of Eq. (56) is taken at the point $\lambda = \lambda_1 \equiv \lambda_*$ of the spectrum: $\widehat{L} = \widehat{L}(\lambda_*)$. In such a case, the condition allowing Eq. (56) to have a nontrivial solution represents a requirement that its right-hand part is orthogonal to the eigenfunction $\boldsymbol{\Psi}_*$ [77]. This yields the equation

$$(a - a_*)\xi^i I_2^i + b_3 \sum_{j,k=1}^{n} \gamma_3^{ijk} I_3^{ijk}\xi^j\xi^k + b_4^{(0)} \sum_{j=1}^{n} I_4^{iijj}\xi^i(\xi^j)^2 + \sum_{j,k,l=1}^{n} R^{ijkl}\xi^j\xi^k\xi^l = 0, \tag{57}$$

where

$$R^{ijkl} = -\Lambda^{ijkl} + \sum_{s=1}^{m_4} b_4(s)\gamma^{ijkl}(s)I_4^{ijkl}$$

while I_2^i, I_3^{ijkl}, etc., are the integrals:

$$I_2^i = \int (\Psi_*^i)^2 d\Omega;\ I_3^{ijk} = \int \Psi_*^i\Psi_*^j\Psi_*^k d\Omega;$$
$$I_4^{ijkl} = \int \Psi_*^i\Psi_*^j\Psi_*^k\Psi_*^l d\Omega \tag{58}$$

while

$$\Lambda^{ijlm} = \int K^{ijlm}(\mathbf{k},\mathbf{k}\cdot\mathbf{V})q^{ij}(\mathbf{k})q^{lm}(-\mathbf{k})\frac{d^2k}{(2\pi)^2},$$

where $q^{ij}(\mathbf{k})$ is the Fourier transform of the product $\Psi_*^i(\mathbf{r})\Psi_*^j(\mathbf{r})$:

$$q^{ij}(\mathbf{k}) = \int \Psi_*^i(\mathbf{r})\Psi_*^j(\mathbf{r})\exp(-i\mathbf{k}\cdot\mathbf{r})d^2r. \tag{59}$$

The equations (57) are referred to as the *ramification equations*. They constitute a system of algebraic equations of the third order on the set of the amplitudes ξ and its solution enables one to find the values of the amplitudes and to build the bifurcation diagram. The latter defines the regions of existence of the zones of different kinds in the space of parameters a and b_s.

It should be mentioned that the ramification equations depend on the constants a, a_*, and b_s as well as on the integrals J_2^i, J_4^{ijkl}, and Λ^{ijkl}. The latter in turn depend on the eigenfunctions, which are assumed to be known, as well as on the elastic Green's function. One concludes that (57) represents a closed system of algebraic equations with explicitly specified coefficients.

One observes that Eq. (57) can be obtained as a condition of a minimum of a generating function F_{eff}:

$$F_{\text{eff}} = \frac{(a - a_*)}{2}\sum_{i=1}^{n} I_2^i(\xi^i)^2 + \frac{b_3}{3}\sum_{i,j,k=1}^{n}\gamma_3^{ijk}I_3^{ijk}\xi^i\xi^j\xi^k + \frac{1}{4}\sum_{i,j,k,l=1}^{n}\left(b_4^{(0)}I_4^{ijkl}\delta^{ij}\delta^{kl} + R^{ijkl}\right)\xi^i\xi^j\xi^k\xi^l \tag{60}$$

with respect to ξ^i. To avoid misunderstanding, we stress that the propagating zone is not in the equilibrium state and cannot be described by the minimization of the Landau potential. However, technically, the ramification equations can be derived from the generating function (60) in exactly the same way as the state equation is derived from the conventional Landau potential in the Landau theory [35]. We, therefore, refer to (60) as the *effective Landau potential* of the process zone.

C. Classification of the types of zones

Equations (57) constitute a system of n algebraic equations. These admit the trivial solution $\xi^i = 0$ for all $i = 1,\ldots,n$, describing no zone. In addition, it may have nontrivial solutions of various types. The classification of the possible zone types can be done as follows.

First, one can find one-parametric zones, such as (A) $\boldsymbol{\xi} = (\xi,0,0,\ldots,0)$, (B) $\boldsymbol{\xi} = (\xi,\xi,0,\ldots,0)$, (C) $\boldsymbol{\xi} = (\xi,\xi,\xi,\ldots,0)$, and so on, and, finally, (D) $\boldsymbol{\xi} = (\xi,\xi,\xi,\ldots,\xi)$. Here, $\xi \neq 0$ is a solution of (57). From experience, one can expect that the one-parametric zone structures, such as (A), (B), (C), ...(D), often (though not always) show up first, while the multiparametric structures [such as $\boldsymbol{\xi} = (\xi_1,\xi_2,\xi_3,\ldots,0)$, where $\xi_1 \neq \xi_2 \neq \xi_3$ etc.] are often absent in the phase diagram.

It should be noted that if the group $\mathfrak{G}$ admits the cubic invariant (2), the bifurcation is only soft under the condition $b_3 = 0$. Since the coefficient b_3 is generally a function of the thermodynamic variables, the above condition together

with $T = T_*$ yields a point on the phase diagram where the bifurcation is soft, while in its vicinity the bifurcation is close to a soft one. In contrast, if the cubic invariant (2) is forbidden by the symmetry, one only finds the second- and fourth-order terms in the effective Landau potential. It is this case that will be analyzed here.

As an example, let us analyze the one-parametric structures. In this case, the effective Landau potential (60) and ramification equations (57) take the forms

$$F_{\text{eff}} = \frac{(a-a_*)}{2}\xi^2 \sum_{i=1}^{n} I_2^i + \frac{b}{4}\xi^4, \tag{61}$$

$$(a-a_*)\xi \sum_{i=1}^{n} I_2^i + b\xi^3 = 0, \tag{62}$$

where in case (A) one finds $b = b_A$,

$$b_{\text{A}} = b_0 I_4^{1111} + R^{1111}, \tag{63}$$

while in case (D),

$$b_{\text{D}} = b_0 \sum_{i,j=1}^{n} I_4^{iijj} + \sum_{i,j,k,l=1}^{n} R^{ijkl}. \tag{64}$$

The cases of the other one-component combinations (B), (C), and so on can be described by Eq. (62) with the only difference being in the expression for b.

One finds the order parameter amplitude:

$$\xi = \begin{cases} 0, & a > a_* \\ \pm\sqrt{\left[(a_*-a)\sum_{i=1}^{n} I_2^i\right]/b}, & a \leqslant a_*. \end{cases} \tag{65}$$

As expected, one concludes that the zone emerges at $a = a_*$ [Eq. (55)] and the dependence $\xi = \xi(a)$ is continuous, though not smooth. The question of which zone emerges first can be solved by substituting the solution (65) into the effective Landau potential (61), yielding

$$F_{\text{eff}} = -\frac{(a_*-a)^2\left(\sum_{i=1}^{n} I_2^i\right)^2}{4b} < 0 \tag{66}$$

representing, at least in the case of a motionless crack, the energy gain due to the bifurcation. One concludes that F_{eff} is smaller in the case of the zone with the smallest b. Therefore, it is the one-parametric zone with the smallest b that emerges earlier than the other one-parametric zones. However, since b_0 and R^{ijkl} may depend on the thermodynamic parameters, the solutions with the smallest b may be different in different parts of the phase diagram. This question should be solved separately for specific cases. Further, the question is still not solved completely since we did not analyze the multiparametric zones.

Other zone types can be analyzed in an analogous way. One should take into account that Eq. (57) minimizes the effective Landau potential (60). This enables one to make use of the necessary and sufficient conditions of its minimum in terms of the second derivatives, as well as taking into account possible transformations of the different zones into one another. However, the analysis of the other zones in a general form includes much too lengthy expressions. It can be reasonably easily done, however, in specific cases.

V. DISCUSSION

A. Eigenfunction and eigenvalues

We have shown that provided the generalized Schrödinger equation (53) has at least one point a_* in the discrete spectrum, Eqs. (40) have a bifurcation at $a = a_*$ [Eq. (55)]. The arguments of this paper are based on the expectation that such a discrete spectrum exists, and its first eigenvalue λ_* and eigenfunction $\psi_*(\rho,\theta)$ are known. In such a situation, it is important to give examples of solutions (53) exhibiting such a discrete spectrum. A few such examples are briefly described below.

1. Dilatation-dominated spontaneous strain

Spontaneous dilatation $Q^{ij}_{\alpha\beta} = Q_0\delta_{\alpha\beta}\delta^{ij}$ is always present in the potential Φ_{int} [Eq. (12)] since the term $\sigma_{\alpha\alpha}\sum_{i=1}^{n}(\eta^i)^2$ is invariant with respect to all crystallographic groups. If the symmetry group forbids other mixed terms, only the spontaneous dilatation is present in the process zone. Further, in some materials the off-diagonal spontaneous strain terms are allowed by symmetry, but they are much smaller than the dilatation. Both cases correspond to a spontaneous strain dominated by the dilatation.

As our first example, let us consider an elastically isotropic solid with a dilatation-dominated process zone. The elastically isotropic approximation is a good one for, e.g., most cubic metals [78]. Using well-known results of the fracture theory for the stress distribution at the crack tip [79], one finds the tensor $\varphi_{\alpha\beta}(\theta)$ (41) in the form

$$\begin{gathered} \varphi_{11,22} = \cos(\theta/2)[1-2\sigma \mp \sin(\theta/2)\sin(3\theta/2)]; \\ \varphi_{12} = \varphi_{21} = \cos(\theta/2)\sin(\theta/2)\cos(3\theta/2), \end{gathered} \tag{67}$$

where the sign "+" corresponds to φ_{11}, while "−" corresponds to φ_{22}. This yields $U^{ij}(\rho,\theta) = \delta^{ij}U_0(\rho,\theta)$, with $U_0(\rho,\theta) = \cos(\theta/2)/\sqrt{\rho}$, and the spectral equations (53) take the form

$$\Delta\psi_p^i \mp \frac{\cos(\theta/2)}{\sqrt{\rho}}\psi_p^i = \lambda_p\psi_p^i \tag{68}$$

equal for all $i = 1,\ldots,n$. The sign "−" corresponds to $Q_0 > 0$, while the sign "+ "is taken in the opposite case. Figure 2(a) shows the potential $-U_0(\rho,\theta)$, that is, in the case of the sign "+" representing a potential well. In the opposite case, it represents a "hill." Therefore, a discrete spectrum only exists if the sign $Q_0 < 0$. In this case, it consists of a single spectral point $p = 1$. The corresponding eigenfunctions are equal to one another for all values of i $(i = 1,\ldots,n)$: $\psi_*^i \equiv \psi_*$ and $\Psi_*^i \equiv \Psi_*$. The exact solution of the eigenproblem has been presented elsewhere [39]. The eigenfunction ψ_* is shown in Fig. 2(b). The exact solution yields the eigenvalue $\lambda_* = 2^{-1} \times 2^{-1/3}$, which is approximately equal to 0.4.

The case $Q^{ij}_{\alpha\beta} = Q_0\delta_{\alpha\beta}\delta^{ij}$ takes place, e.g., in superconductors such as Sn, Pb, Fe [1], Nb, and Ta [50], and superconductive compounds C_6Ca [51], $C_{60}K_3$ [52].

2. Shear-dominated spontaneous strain

Some materials exhibit a shear spontaneous strain considerably exceeding the spontaneous dilatation. For example, $\varepsilon^{(0)}_{xy}$ is fourfold greater than $\varepsilon^{(0)}_{\alpha\alpha}$ in ZrO_2 [80]. In order to

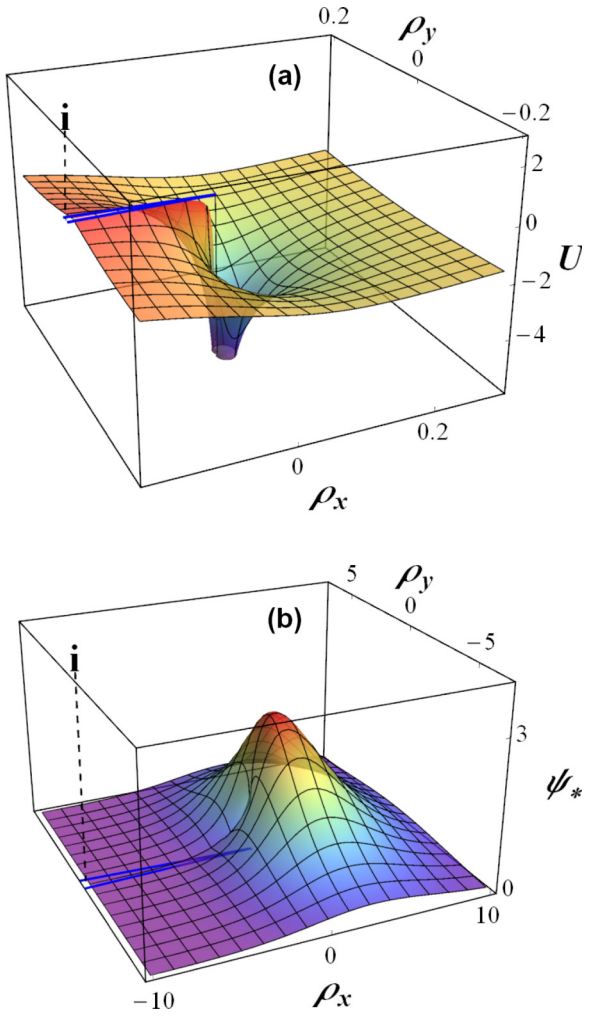

FIG. 2. (a) Example of the potential $U^{ij}(\rho_x,\rho_y) = U(\rho_x,\rho_y)\delta^{ij}$ in the elastically isotropic and purely dilatant case. (b) The eigenfunction $\psi_*(\rho_x,\rho_y)$ as the functions of the Cartesian coordinates $\rho_x = \rho\cos(\theta)$ and $\rho_y = \rho\sin(\theta)$. (i) indicates the crack-tip position.

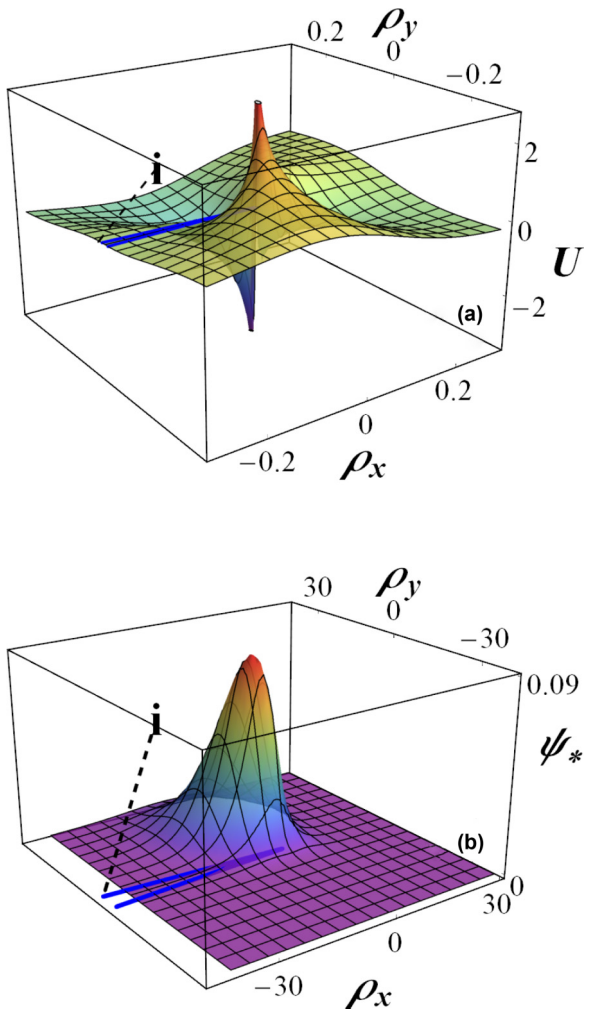

FIG. 3. Potential $U_1(\rho_x,\rho_y)$ (a) and the eigenfunction $\psi_*(\rho_x,\rho_y)$ (b) at the tip of the crack with the shear spontaneous strain at $Q_1 > 0$. (i) indicates the crack-tip position.

educe its consequences, let us consider a shear-dominated spontaneous strain in an elastically isotropic solid as our next example. The potential $U^{ij}(\rho,\theta)$ [Eq. (54)] is determined by $Q^{ij}_{\alpha\beta} = (Q_0\delta_{\alpha\beta} + Q_1\delta_{\alpha 1}\delta_{\beta 2})\delta^{ij}$ and we assume $|Q_1| \gg |Q_0|$, neglecting the spontaneous dilatation. Using (67), one finds $U^{ij}(\rho,\theta) = \delta^{ij}U_1(\rho,\theta)$, where $U_1(\rho,\theta) = \sin(\theta/2)\cos(\theta/2)\cos(3\theta/2)/\sqrt{\rho}$ [Fig. 3(a)]. The spectral equation takes the form

$$\Delta\psi^i_p \mp \frac{\sin(\theta/2)\cos(\theta/2)\cos(3\theta/2)}{\sqrt{\rho}}\psi^i_p = \lambda_p\psi^i_p, \qquad (69)$$

the same for all $i = 1,2,\ldots,n$. Here again the signs "+" and "−" correspond to $Q_1 > 0$ and $Q_1 < 0$. The solutions for the eigenvalue, $\lambda_* \approx 0.084$, and the eigenfunction [shown in Fig. 3(b)] have been obtained numerically. Details of the numerical solution are given in Appendix A.

It should be noted that the eigenfunction $\psi_*(\rho_x,\rho_y)$ is asymmetric. It is located at one side of the crack tip and is shifted a bit backwards [Fig. 3(b)]. The solution in the case $Q < 0$ can be obtained from the one shown in Fig. 3(b) by reflecting it in the plane $y = 0$. The striction term $Q^{ij}_{\alpha\beta} = (Q_0\delta_{\alpha\beta} + Q_1\delta_{\alpha 1}\delta_{\beta 2})\delta^{ij}$ takes place, for example, during the structural phase transition in VO_2 describing by the four-component order parameter from the D^{14}_{4h} phase into the C^5_{2h} and C^3_{2h} ones. In the first case, the mixed invariant $[(\eta^1)^2 + (\eta^2)^2]\varepsilon_{xy}$, while in the second one $(\eta^1)^2\varepsilon_{xy}$ takes place [43,65]. It also takes place in some langbeinites, such as during the transition $T^4 \to C^2_2$ in $TlCd_2(SO_4)_3$ [81], boracites, such as during the transition $T^5_d \to C^5_{2v}$ in $Ni_3B_7O_{13}J$ [67], in some perovskites, such as $CsPbCl_3$, and in many other materials.

3. *Concerted effect of elastic anisotropy, dilatation, and shear spontaneous strain*

In the two examples above, we only analyzed an elastically isotropic solid. This has been done for the obvious reason of its mathematical simplicity. The question, however, arises, as to what effects might be introduced by an elastic anisotropy combined with both diagonal and off-diagonal spontaneous stresses? This case can only be addressed numerically, and it is, therefore, reasonable to take some specific solid as an example,

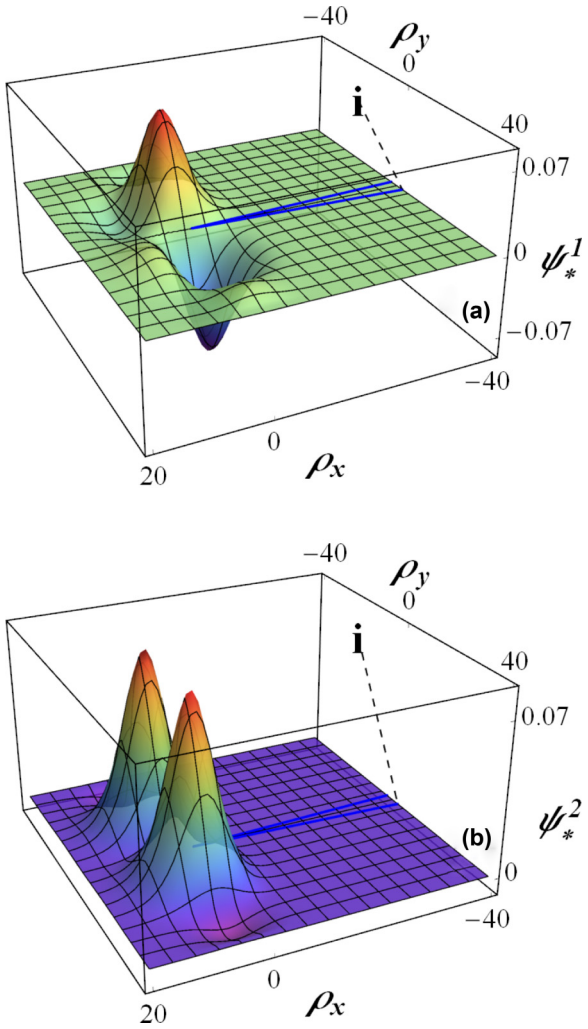

FIG. 4. The eigenfunctions for the case of the $BaTiO_3$. (a) Shows the function $\psi_*^1(\rho_x,\rho_y)$, while (b) represents $\psi_*^2(\rho_x,\rho_y)$. (i) indicates the position of the crack tip.

and to use the numeric values of its elastic and striction constants. For this purpose we have chosen $BaTiO_3$. At atmospheric pressure, $BaTiO_3$ exhibits five phases: hexagonal, cubic, tetragonal, orthorhombic, and rhombohedral [1]. At atmospheric pressure, the transition from the mother cubic phase to the tetragonal phase takes place at 394 K, to the orthorhombic at 284 K, and to the rhombohedral at 200 K. The phase diagram of $BaTiO_3$ can be found in [82]. The phase transitions between the cubic, tetragonal, orthorhombic, and rhombohedral phases are described by a three-component order parameter $\boldsymbol{\eta} = (\eta^1,\eta^2,\eta^3)$ associated with the polarization vector $P_x = \eta^1$, $P_y = \eta^2$, and $P_z = \eta^3$.

We assume $BaTiO_3$ to be in the cubic mother phase and choose a (0,0,1) crystallographic plane as the (x,y) plane, with the crack in the plane $y = 0$ along the positive Ox direction with its tip at the point (0,0). The plane stress problem is considered. Details of the numerical calculations are given in Appendix B. They yield $\lambda_* \approx 0.626$ and the eigenfunction $\boldsymbol{\psi}_*$, only exhibiting the first two nonzero components: $\boldsymbol{\psi}_* = (\psi_*^1,\psi_*^2,0)$. They are shown in Fig. 4.

It should be noted that although we used here the numerical data for $BaTiO_3$ qualitatively, the same results should be expected in the other cubic materials with the three-component order parameter and the same structure of the striction terms, such as $PbTiO_3$, $Pb(Zr_xTi_{1-x})O_3$ [59], in ferromagnetics $Tb_{1-x}Ho_xFe_2$ and $Tb_{1-x}Dy_xFe_2$ [58], and some others.

4. Eigenvalue problem: Concluding remarks

Above we presented a few cases in which the eigenproblem indeed has a solution in the discrete spectrum. For the existence of such a part of the spectrum, it is necessary that at least one of the potentials $U^{ij}(\rho,\theta)$ [Eq. (54)] represent a potential well rather than a hill. Apart from this necessary condition, however, there is no approach to predict whether a discrete spectrum exists or not. According to Eq. (50), the form factor $\boldsymbol{\Psi}(\mathbf{r},t)$ defines the order parameter distribution in the vicinity of the tip of a propagating crack, while $\boldsymbol{\psi}(\mathbf{r})$, related to the latter by Eq. (52), yields that for the vicinity of a motionless crack tip.

One finds that in the elastically isotropic, dilatant case, the eigenfunction is distributed in front of the crack tip, and it is symmetric with respect to the crack plane $y = 0$ [Fig. 2(b)]. We would like to note that it is this case that has been analyzed in detail within the "mechanical" approach, pioneered by Budiansky and coauthors [83]. In particular, their approach differs from ours by assuming the phase boundary to be atomically sharp. They have discovered that the dilatation-dominated zone imposes no direct screening effect on the fracture toughness. The fracture toughness effect has been later attributed to the metastable wake [84]. In our approach, the phase boundary has a finite thickness and a direct screening effect of the zone takes place. It is proportional to the phase boundary thickness, however, and in the case of a narrow interface its impact is small.

In contrast to this, in the shear-dominated, elastically isotropic case, the eigenfunction $\psi_*(\rho_x,\rho_y)$ is asymmetric. It is located at one side of the crack tip and is shifted a bit backwards [Fig. 3(b)], thus imposing a direct impact on one of the crack surfaces. This gives rise to a secondary shear contribution in the plane opening crack mode, and may cause a deflection of the direction of the crack propagation.

The case of crystal $BaTiO_3$ is the most complex one. It should be kept in view that this material exhibits bulk phase transitions of the first order, though they are rather close to second-order ones. For this reason, Eq. (50) only roughly describes the order parameter distribution. One should, therefore, consider this example as a qualitative rather than as a quantitative prediction for $BaTiO_3$.

With this in mind, let us note that in the configuration considered, applying the plane stress, one finds that the eigenfunction component ψ_*^1 is antisymmetric, while ψ_*^2 is symmetric with respect to the crack plane (Fig. 4), while $\psi_*^3 = 0$. One concludes that the P_x polarization component is antisymmetric, while P_y is symmetric and P_z does not exist in the zone of such a crack. It should be stressed that although the P_x distribution looks like two different domains, in fact this is not the case. Division into domains occurs in order to minimize the total free energy accounting for the contribution of the electric field in addition to the elasticity. In contrast, in

the present case, we did not account for the electric field at all. The antisymmetricity is, therefore, a specific property of the zone configuration caused by the peculiarities of the order parameter and the stress distribution itself.

One can see that the distributions are shifted backwards from the crack tip (Fig. 4). This means that the zone exerts forces directly on the crack surfaces close to the tip, where these forces have a strong impact on the stress intensity factor. Again, the antisymmetricity of ψ_*^1 may cause these forces to be applied with different magnitudes to the two different surfaces, which can be controlled by the electric field applied along Ox. As in the case of the shear-dominated process zone discussed above, this can give rise to a number of nontrivial effects. These are, however, outside the scope of this paper.

Let us note that the above results are only valid provided the discrete spectrum of Eq. (53) does indeed exist. Here, only the value of the dimensionless spectral number λ_* depends on the details of the system, such as the structure of the deviatoric terms fixed by the dimensionless coefficients $B^{ij}(\theta)$ or the elastic moduli $\mathbf{C}$. One cannot predict the value of λ_* without explicitly solving Eq. (53).

If (i) all components $B^{ij}(\theta) < 0$ and (ii) the solution corresponding to the discrete spectrum exists, the zone emerges at $T_* \geqslant T \geqslant T_c$, that is above the line of the bulk phase transition on the phase diagram. In the opposite case, $B^{ij}(\theta) > 0$, the zone emerges below rather than above the bulk transition point $T_c \geqslant T \geqslant T_*$, as we have demonstrated elsewhere in the one-component case [39]. Finally, if $B^{ij}(\theta)$ as a function of the angle θ changes its sign, the zone may emerge both above and below the bulk transition, at $T_{*1} \geqslant T \geqslant T_{*2}$, where $T_{*1} > T_c > T_{*2}$. In this case, the spatial configurations of the zones below and above the bulk transition line in general differ from one another. Typically, values of λ_* between 0.01 and 1 are to be expected.

B. Process zone emergence temperature

As is usually done in the Landau theory of phase transitions [35], assuming $a = a_0(T - T_c)$ and observing that $a_* = a_0 \Delta T_*$, where $\Delta T_* = T_* - T_c$, one finds

$$\Delta T_*(K_I) = \frac{\lambda_*}{a_0 g^{1/3}(2\pi)^{2/3}}(QK_I)^{4/3} - \frac{\kappa^2 V^2}{4 g a_0}. \tag{70}$$

C. Critical velocity

The zone emerges at $a \leqslant a_*$, where the nontrivial solutions branch off from the trivial one. Since at $a < 0$ the transition to the bulk low-symmetry phase occurs, one concludes that the process zone only exists within the interval $0 \leqslant a \leqslant a_*$. Since at $a_* = 0$ the process zone vanishes, this condition, together with Eq. (55), defines a critical velocity V_*:

$$V_*(K_I) = \left(\frac{4}{\pi}\right)^{1/3} \frac{\lambda_*^{1/2} g^{1/3}}{\kappa}(QK_I)^{2/3}. \tag{71}$$

The crack tip can only be dressed for $V \leqslant V_*$.

D. Dynamic phase diagram

Equation (71) by itself is incomplete since the velocity V depends on the stress intensity factor K_I according to the equation of crack propagation put forward by Freund [85], yielding

$$V = V_R\left(1 - K_{IC}^2/K_I^2\right), \tag{72}$$

where V_R is the Rayleigh velocity. Together with (70), this enables one to find the condition that a bare crack tip becomes unstable with respect to the zone emergence. Inserting (72) into (70), one finds the zone emergence condition

$$\frac{\Delta T}{\Delta T_{*0}} = \begin{cases} \left(\frac{K_I}{K_{IC}}\right)^{4/3}, & K_I \leqslant K_{IC} \\ \left(\frac{K_I}{K_{IC}}\right)^{4/3} - \frac{1}{\nu^2}\left(1 - \frac{K_{IC}^2}{K_I^2}\right)^2, & K_I > K_{IC} \end{cases} \tag{73}$$

where $\Delta T = T - T_c$, and the dimensionless parameter ν has the form

$$\nu = \frac{V_*(K_{IC})}{V_R} = \left(\frac{4}{\pi}\right)^{1/3} \frac{\lambda_*^{1/2} g^{1/3}}{\kappa V_R}(QK_{IC})^{2/3}. \tag{74}$$

Equation (73) defines the dynamic phase diagram of the process zone in terms of the stress intensity factor K_I and the temperature T. In the interval $0 \leqslant K_I \leqslant 2K_{IC}$, it is shown in Figs. 5(a)–5(c) in terms of the dimensionless coordinates K_I/K_{IC} and $\Delta T/\Delta T_{*0}$. It includes a motionless crack at $0 \leqslant K_I \leqslant K_{IC}$ and one at the beginning of its motion at $K_{IC} \leqslant K_I \leqslant 2K_{IC}$.

In the case of a propagating crack ($K_I > K_{IC}$), however, it is more convenient to graph the ratio $\Delta T/\Delta T_{*0}$ against $1 - K_{IC}^2/K_I^2$ [Figs. 5(d)–5(f)]. The latter variable changes from 0 to 1 when K_I varies from K_{IC} to infinity. Figure 5 shows the phase diagram both against K_I/K_{IC} [Figs. 5(a)–5(c)] and $1 - K_{IC}^2/K_I^2$ [Figs. 5(d)–5(f)] for $\nu = 0.3$, 0.5, and 0.9, exhibiting different phase diagram configurations.

In region I there is no process zone at the crack tip, but it exists in region II. The latter is shaded in Fig. 5. Let us note that at any temperature there is a region II where the process zone exists. However, in the case of small and intermediate values of ν, the zone emergence line (73) exhibits a maximum to the right of the point $K_I = K_{IC}$. It is indicated by the letter "M" in Fig. 5 and the corresponding value of the temperature is T_M with a temperature shift $\Delta T_M = T_M - T_c$. If the temperature shift exceeds ΔT_M, the zone can only show up at crack speeds close to the Rayleigh velocity, as in the case shown in Figs. 5(a) and 5(d). In the latter case, it takes place as soon as the boundary of the region II b is reached. Achieving such a velocity requires a high value of K_I, which may appear experimentally unattainable. In addition, in this case the zone accompanies the crack moving with a high speed, which makes its observation difficult. In such a situation, the zone can only be observed for $\Delta T < \Delta T_M$.

Note that in the case of small and intermediate values of ν, Figs. 5(a) and 5(d) as well as 5(b) and 5(e) for $\Delta T < \Delta T_M$, there is the possibility, that with an increasing stress intensity factor, the zone emerges and then vanishes. Finally, in the case shown in Figs. 5(c) and 5(f), once the zone has formed, it never vanishes with increasing K_I.

Let us note that we only discussed the dressing condition here. The undressing condition is more complex and will not be discussed in this paper. We refer the reader to [38], where it is studied in the case of a one-component order parameter.

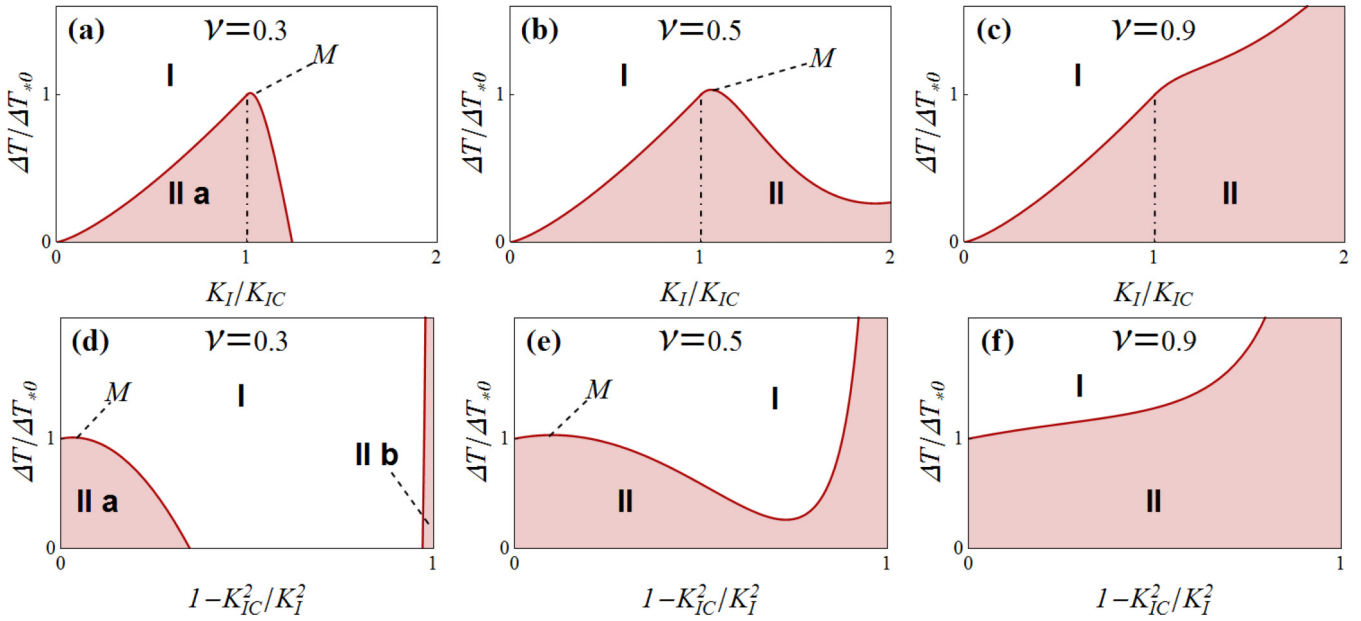

FIG. 5. Phase diagram of the process zone in the plane (K_I, T) exhibits two regions: I with no zone at the tip and II where the crack is dressed. (a)–(c) Show the phase diagram at $0 \leqslant K_I \leqslant 2K_{\rm IC}$ with $\nu = 0.3$, 0.5, and 0.9 correspondingly. The dotted-dashed line separates the phase diagram part with the motionless crack (left) from that with the propagating one (right). (d)–(f) Show the phase diagram for a propagating crack at $K_{\rm IC} \leqslant K_I < \infty$, as a function of $1 - K_{\rm IC}^2/K_I^2$. M indicates the point of maximum of the zone emergence line (if any).

It should also be stressed that the above result is valid for any zone at any crack, provided Eq. (53) has a solution in the discrete spectrum. One concludes that the expressions for the boundary of the zone emergence (73) and of the emergence temperature (70) are universal.

E. Estimates

Let us estimate the zone emergence temperature $\Delta T_* = \Delta T_*(K_I, V)$ [Eq. (70)] at the tip of a motionless crack, $V = 0$. The temperature $\Delta T_{*0} = \Delta T_*(K_{\rm IC})$ describes the emergence of a zone at the tip of a motionless crack at the threshold value $K_I = K_{\rm IC}$ of the stress intensity factor. It only depends on the material constants and, therefore, it itself can be regarded as a material constant. One can represent ΔT_{*0} as follows:

$$\Delta T_{*0} \sim \lambda_* (k K_{\rm IC})^{4/3} r_{\rm c0}^{-2/3}. \tag{75}$$

Here, we used the observation that up to a numerical factor the striction tensor norm Q is related to the slope $k = dT_{\rm c}(p)/dp$ of the phase diagram line $T_{\rm c} = T_{\rm c}(p)$ by $Q \sim a_0 k$, where p is the hydrostatic pressure. Further, $r_{\rm c0} = (g/a_0)^{1/2}$ is the order parameter correlation radius 1 K away from the bulk transition line.

The form (75) is convenient for making estimates. The lines of the phase transitions on the phase diagrams of solids may possess any slope, typical values being in the range $k \sim (0.1\text{–}10) \times 10^{-8}\,{\rm cm^3\,K\,/\,erg}$ [1]. Most inorganic solids have a correlation radius $r_{\rm c0} \sim 1$ nm $\rm K^{1/2}$ [86] and $K_{\rm IC} \sim 10^8$ erg $\rm cm^{-5/2}$ [87]. Assuming $\lambda_* \sim$ 0.1 to 1, one finds the estimate $|\Delta T_*(K_{\rm IC})| \sim 10$ to 10^2 K.

Observing that the entire phase diagram of an inorganic solid lies between 0 and ∼1000 K, the above estimate leads to our most striking conclusion: the transformational process zone accompanies, with a high probability, a brittle fracture of an inorganic solid, existing in a considerable part of the solid phase diagram. As we have seen, the form of the dynamic phase diagram (Fig. 5) critically depends on the value of the dimensionless parameter ν. Let us give numerical estimates of this parameter for a few materials.

For $BaTiO_3$, the values of the fracture toughness, depending on the porosity, vary from $K_{\rm IC} \approx 0.56 \times 10^8$ to 2.3×10^8 erg $\rm cm^{-5/2}$ [88], $Q \approx 1.47 \times 10^{-12}\,{\rm cm^3\,/\,erg}$ [59], $\kappa \sim 10^{-14}$ s [89], $g \sim 10^{-16}\,{\rm cm^2}$ [90], and the Rayleigh velocity as $V_{\rm R} \approx 0.9(E/\rho)^{1/2} \approx 3.7 \times 10^5$ cm / s, one finds $\nu \approx 0.5$ to 1.2 depending on the value of $K_{\rm IC}$.

An analogous estimate for $PbTiO_3$ with $K_{\rm IC} \approx 1.38 \times 10^8$ erg $\rm cm^{-5/2}$[91], $\kappa \sim 10^{-14}$ s $g \sim 10^{-16}\,{\rm cm^2}$ [90], $Q \approx 1.27 \times 10^{-12}\,{\rm cm^3\,/\,erg}$ [59], and with $V_{\rm R} = 0.9(E/\rho)^{1/2} \approx 3.6 \times 10^5$ cm / s yields $\nu \approx 0.8$.

To estimate the zone size $R_{\rm z}$, let us first note that it does not coincide with the characteristic scale R [Eq. (51)]. Indeed, R yields the thickness of the phase interface, while the zones obtained above exhibit sizes 30 to 40 times greater. Let us, therefore, take the estimate $R_{\rm z} \sim 10R$:

$$R_{\rm z} \sim 10\left(\frac{r_{\rm c0}^2}{k K_I}\right)^{2/3}. \tag{76}$$

At the threshold point $K_I = K_{\rm IC}$, one finds the size of the newborn zone $R_{\rm zc} \sim 1$ to 10 nm. Figure 6 shows the dependence of the zone size on the stress intensity factor $0 \leqslant K_I \leqslant K_{\rm IC}$, assuming $R_{\rm zc}(K_{\rm IC}) = 1$ nm.

F. On the difference between the "mechanical" and the Ginzburg-Landau approaches

The approach developed here regards the order parameter $\boldsymbol{\eta}$ as a primary characteristic of the process zone, while the spontaneous strain field is considered as a secondary

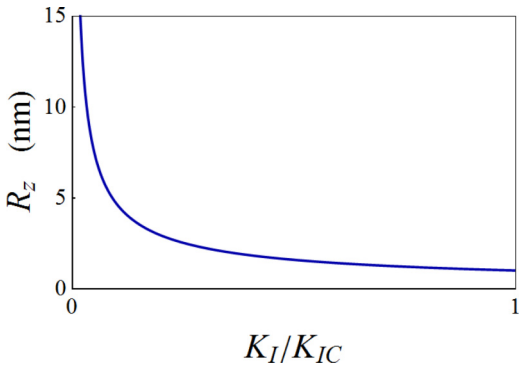

FIG. 6. Dependence of the process zone size on the stress intensity factor. Parameters of the formula (76) correspond to the estimates given above.

characteristic. The bifurcation is associated with a certain energy gain, as we have seen in Eq. (66). It can only take place if this gain is high enough to overcome the resistance of the solid caused by the corresponding growth of its elastic energy. This conclusion is borne out by the observation of zones (e.g., [6]) exhibiting lattice structures different from that of the strained mother phase, but requiring a complex rearrangement of the elementary cell [92].

At a point lying far away from the crack tip, the order parameter is zero. As soon as the zone at the crack tip approaches this point, the order parameter gradually grows from zero to some value. Such an internal zone dynamics has a considerable impact on the crack's motion [38].

One should, however, note that some materials exhibit pronounced first-order transitions. That is, at the transition point, the order parameter makes a jump to a value close to that of its saturation and does not significantly vary further. Although zones in these materials still can be characterized by the order parameter, the approach of this paper has to be significantly modified for these cases. It is clear, however, that such an almost saturated order parameter exhibits a weak internal dynamics, while the zone is mainly described by the configuration and dynamics of its boundary.

In contrast to our approach, the "mechanical" one ignores any degrees of freedom except for the elastic ones and characterizes the zone by the phase boundary configuration [3]. One concludes that it is "designed" to describe a zone characterized by a pronounced first-order phase transition.

VI. SUMMARY

We addressed the emergence of a transformational process zone at a crack tip. We have argued that the zone should be described by an n-component order parameter $\boldsymbol{\eta}$, responsible for the differences in symmetry and structure between the process zone and the bulk of the solid. It interacts with the strain field and its dynamics obeys a system of generalized, time-dependent Ginzburg-Landau equations, while the strain is subjected to the mechanical equations of motion.

By eliminating the elastic variables, we derived a system of n equations for the components of the order parameter, describing its dynamics in response to a solid loading. This derivation has been kept in the most general form and is applicable to any solid whose process zone is described by an n-component order parameter. We, further, reduced this system to one describing a traveling inhomogeneity in the solid, such as a propagating crack, dislocation, a sound or shock wave, etc.

We, finally, specialized to a steadily, rectilinearly propagating crack. In this latter case, we analyzed a point of bifurcation of the equations and derived the ramification equations for the amplitudes of the emerging solutions, enabling one to describe the structure of the process zone below the bifurcation point. We, thus, demonstrated that the formation of a transformational process zone at the tip of a crack in a brittle solid takes place by way of a bifurcation. We also demonstrated that it takes place, provided the spectral equation (53) has a solution in the discrete spectrum. Assuming that this condition holds, we described the bifurcation in the most general case.

In particular, we have shown that the formation of a transformation process zone exhibits *universal* features: the temperature of the zone emergence $\Delta T_* = T_* - T_c$ universally scales with K_I as $\Delta T_* \sim K_I^{4/3}$, and that the zone vanishes upon achieving a critical velocity $V_* \sim K_I^{2/3}$. We, further, built a universal dynamic phase diagram describing the emergence and vanishing of the zone at the tip of a propagating crack.

ACKNOWLEDGMENT

The research of A.L.K. was supported by the Russian Foundation of Basic Reseach (RFBR) under Grant No. 16-01-00068-a and RFBR Grant No. 17-02-00365, and Yu.M.G. was partially supported by South Federal University (Russia) through the University Development Fund, Grant No. 6386.2017/BC.

APPENDIX A: NUMERICAL SOLUTION OF THE EIGENPROBLEM IN THE SHEAR-DOMINATED CASE

The spectral equation (69) can be solved numerically, employing the following artificial approach. On the basis of bifurcation theory, one concludes that a nonlinear equation

$$\Delta\psi = \left[\lambda \pm \frac{\sin(\theta/2)\cos(\theta/2)\cos(3\theta/2)}{\sqrt{\rho}}\right]\psi + \psi^3 \quad \text{(A1)}$$

of which the linear part coincides with (69) exhibits a bifurcation at the point $\lambda = \lambda_*$. On the basis of the relation (50), one further concludes that its normalized, nontrivial solution taken close to the bifurcation point represents the eigenfunction ψ_*.

Technically, however, this problem is easy to solve considering a pseudodynamic equation

$$\frac{\partial\psi}{\partial\tau} = \Delta\psi - \left[\lambda \pm \frac{\sin(\theta/2)\cos(\theta/2)\cos(3\theta/2)}{\sqrt{\rho}}\right]\psi - \psi^3 \quad \text{(A2)}$$

instead of the stationary one (A1). Here, τ is a pseudotime, the artificial time introduced for the purpose of the numerical method. The dependent variable $\psi = \psi_\lambda(\tau,\rho,\theta)$ is now considered as a function of ρ, θ, the pseudotime τ, and the parameter λ. The calculation employs the fact that as $\tau \to \infty$, Eq. (A2) converges to a fixed point. The latter represents the solution of the stationary equation (A1). The advantage of this approach is that the numerical method of solution

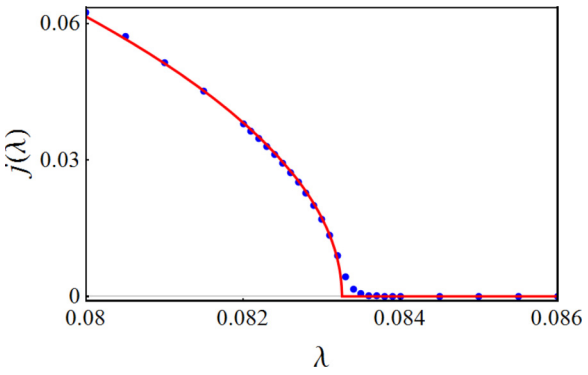

FIG. 7. Seach for the bifurcation point λ_* of the equation (A1). Dots show the results of the numeric simulation, while the solid line represents the fitting.

of (A2) is more stable than that of the linear equation (69) and the nonlinear stationary equation (A1). There is, however, a penalty, since to achieve an acceptable precision one must pursue the numerical method up to high values of τ (see below).

The problem can be solved using the standard NDSolve routine of *Mathematica* 11.0 [93] employing "MethodOfLines" as the method. The problem was solved in Cartesian, rather than in cylindrical coordinates, since it is convenient in the "MethodOfLines" case, enabling one to apply periodic boundary conditions. A square considerably exceeding the characteristic size of the solution was chosen as the domain. The value of ψ on the domain boundary was taken equal to zero.

In order to look for the spectral point λ_*, the solution was normalized with respect to the function obtained at some arbitrarily chosen value of $\lambda = 0.01$ far enough below the bifurcation point: $j(\lambda) = (\int \psi_\lambda^2\, d\Omega / \int \psi_{0.01}^2\, d\Omega)^{1/2}$, where $d\Omega = d\rho_x d\rho_y$. The integrals were evaluated with the help of the standard "NIntegrate" routine of *Mathematica* 11.0 with a local adaptive method, employing an even-odd subdivision strategy. The behavior of $j(\lambda)$ is shown in Fig. 7.

The numerical results were fitted by the function

$$j(\lambda) = \begin{cases} 0, & \lambda > \lambda_* \\ k\sqrt{\lambda_* - \lambda}, & \lambda \leqslant \lambda_* \end{cases} \tag{A3}$$

where k and λ_* are fitting parameters. The fitting yields the spectral value $\lambda_* \approx 0.0833$.

Then, the eigenfunction was taken at $\lambda_0 \approx 0.082$, which is 0.001 below the bifurcation point, and normalized: $\psi_*(\rho_x,\rho_y) \approx \psi_{\lambda_0}(\rho_x,\rho_y)/(\int \psi_{\lambda_0}^2 d\Omega)^{1/2}$, such that $\int \psi_*^2(\rho_x,\rho_y)d\Omega = 1$. It is shown in Fig. 3(b). For the convergence of the solution, the pseudotime value $\tau_{\max} = 10\,000$ was found to be satisfactory at $\lambda_0 = 0.082$. We describe the convergence control in more details at the end of Appendix B.

APPENDIX B: NUMERICAL SOLUTION OF THE EIGENPROBLEM IN THE $BaTiO_3$ CASE

In its mother phase, $BaTiO_3$ is a cubic crystal. Its elastic and striction constants in the mother phase are listed in Table I.

TABLE I. Material constants of $BaTiO_3$ [59].

	C_{1111}	C_{1122}, C_{2211}	C_{1212}
10^{12} erg cm^{-3}	1.78	0.96	1.22
	Q_{11}^{11}	Q_{11}^{22}, Q_{22}^{11}	Q_{12}^{12}
10^{-12} erg^{-1} cm^3	1.22	−0.5	0.656

Let us take the (x,y) plane to coincide with the $(0,0,1)$ crystallographic plane and assume that the crack lies in the plane $y = 0$. In the anisotropic case, the solution of the elastic problem requires to find the roots s_1 and s_2 of the characteristic Lekhnitskii equation [94]. Introducing $k = (C_{1111}^2 - C_{1122}^2)/2C_{1111}C_{1212}$ and using the material constants from Table I one finds $k \approx 0.517$, and the Lekhnitskii equation takes the form

$$s^4 + 2(1+k)s^2 + 1 = 0, \tag{B1}$$

yielding two nonconjugate imaginary solutions: $s_1 \approx 0.6i$ and $s_2 \approx 1.6i$. The solution for the stress tensor in terms of the roots s_1 and s_2 of the Lekhnitskii equation is given in [95]. With its use, one finds the components of $\varphi_{\alpha\beta}(\theta)$ [Eq. (41)]:

$$\varphi_{11} \approx \mathrm{Re}\left[\frac{2.72}{\sqrt{\cos\theta + 1.6i\sin\theta}} - \frac{1.02}{\sqrt{\cos\theta + 0.6i\sin\theta}}\right], \tag{B2}$$

$$\varphi_{22} \approx \mathrm{Re}\left[\frac{2.84}{\sqrt{\cos\theta + 0.6i\sin\theta}} - \frac{1.06}{\sqrt{\cos\theta + 1.6i\sin\theta}}\right],$$

$$\varphi_{12} \approx \mathrm{Re}\left[\frac{1.7i}{\sqrt{\cos\theta + 1.6i\sin\theta}} - \frac{1.7i}{\sqrt{\cos\theta + 0.6i\sin\theta}}\right],$$

and from this one finds the potentials $U^{ij}(\rho_x,\rho_y)$:

$$U^{11} \approx \mathrm{Re}\left[\frac{2.85\sqrt{\rho_x - 0.6i\rho_y}}{\sqrt{\rho_x^2 + 0.36\rho_y^2}} - \frac{3.97\sqrt{\rho_x - 1.6i\rho_y}}{\sqrt{\rho_x^2 + 2.56\rho_y^2}}\right], \tag{B3}$$

$$U^{12} \approx \mathrm{Re}\left[\frac{1.25i\sqrt{\rho_x - 0.6i\rho_y}}{\sqrt{\rho_x^2 + 0.36\rho_y^2}} - \frac{1.25i\sqrt{\rho_x - 1.6i\rho_y}}{\sqrt{\rho_x^2 + 2.56\rho_y^2}}\right],$$

$$U^{21} \approx \mathrm{Re}\left[\frac{1.25i\sqrt{\rho_x - 0.6i\rho_y}}{\sqrt{\rho_x^2 + 0.36\rho_y^2}} - \frac{1.25i\sqrt{\rho_x - 1.6i\rho_y}}{\sqrt{\rho_x^2 + 2.56\rho_y^2}}\right],$$

$$U^{22} \approx \mathrm{Re}\left[\frac{2.84\sqrt{\rho_x - 1.6i\rho_y}}{\sqrt{\rho_x^2 + 2.56\rho_y^2}} - \frac{4.09\sqrt{\rho_x - 0.6i\rho_y}}{\sqrt{\rho_x^2 + 0.36\rho_y^2}}\right],$$

$$U^{33} \approx \mathrm{Re}\left[\frac{0.927\sqrt{\rho_x - 1.6i\rho_y}}{\sqrt{\rho_x^2 + 2.56\rho_y^2}} + \frac{1.01\sqrt{\rho_x - 0.6i\rho_y}}{\sqrt{\rho_x^2 + 0.36\rho_y^2}}\right].$$

The potential U^{33} represents a potential hill, which results in the vanishing of the third component of the vector $\boldsymbol{\psi}$.

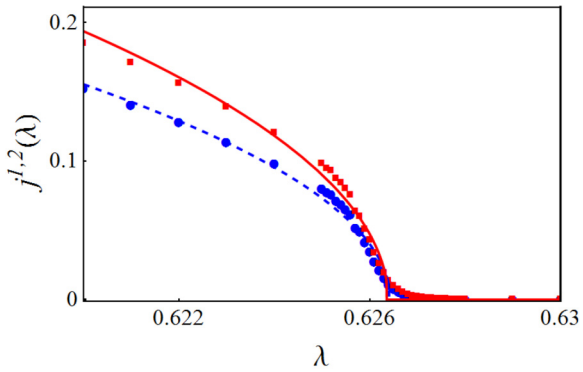

FIG. 8. Search for the bifurcation point λ_* of Eq. (B4). Dots and squares show the results of the numeric simulation of the integrals j^1 and j^2 correspondingly, while the dashed and solid lines represent their fitting.

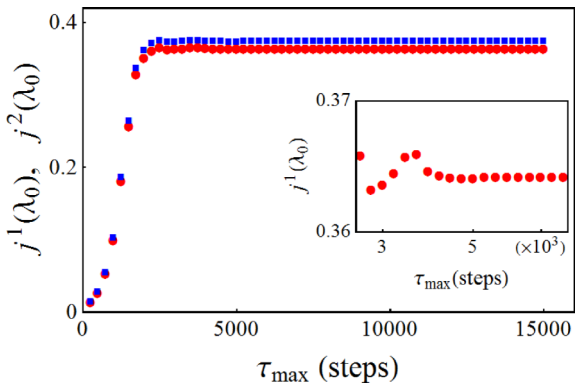

FIG. 9. Convergence control of the numerical process shows the dependence of the integrals $j^i(\lambda_0)$ on the dimensionless simulation time $\tau_{\max}$. Disks show the behavior of $j^1(\lambda_0)$ and squares that of $j^2(\lambda_0)$. The inset demonstrates the behavior of $j^1(\lambda_0)$ in more fine details within the interval $2500 \leqslant \tau_{\max} \leqslant 7000$.

Next, the same approach as the one described in Appendix A was employed. The system of equations has the form

$$\begin{aligned}
\frac{\partial \psi^1}{\partial \tau} &= \Delta\psi^1 - [\lambda + U^{11}(\rho_x,\rho_y)]\psi^1 - U^{12}(\rho_x,\rho_y)\psi^2 - (\psi^1)^3,\\
\frac{\partial \psi^2}{\partial \tau} &= \Delta\psi^2 - [\lambda + U^{21}(\rho_x,\rho_y)]\psi^1 - U^{22}(\rho_x,\rho_y)\psi^2 - (\psi^2)^3,\\
\frac{\partial \psi^3}{\partial \tau} &= \Delta\psi^3 - [\lambda + U^{33}(\rho_x,\rho_y)]\psi^3 - (\psi^3)^3. \qquad \text{(B4)}
\end{aligned}$$

This was solved in the same fashion as described in Appendix A. In this case, there are two functions $\psi^i_\lambda(\tau,\rho,\theta)$ $(i = 1,2)$ depending on ρ, θ, τ, and λ, and we introduce two integrals $j^1(\lambda)$ and $j^2(\lambda)$ defined as follows: $j^i(\lambda) = [\int(\psi^i_\lambda)^2 d\Omega / \int(\psi^i_{0.5})^2 d\Omega]^{1/2}$, where $d\Omega = d\rho_x d\rho_y$. Their behavior is shown in Fig. 8, yielding the eigenvalue $\lambda_* \approx 0.6264$. The eigenfunctions have been calculated at $\lambda_0 = 0.6263$ and normalized: $\psi^i_*(\rho_x,\rho_y) \approx \psi^i_{\lambda_0}(\rho_x,\rho_y)/[\int(\psi^i_{\lambda_0})^2 d\Omega]^{1/2}$.

The control of the convergence of the solution is very important in an applied method. The reason is that equations like (A2) or (B4) have a form analogous to the Landau-Khalatnikov equation [96] with the relaxation time $\tau_c \sim 1/|\lambda - \lambda_*|$, diverging as $\lambda \to \lambda_*$. A reliable result can only be achieved if the pseudotime of the integration $\tau_{\max}$ is a considerable multiple of the relaxation time τ_c.

The control of the convergence was accomplished by observing the saturation of the integrals $j^i(\lambda_0)$ regarded as functions of the maximum time $\tau_{\max}$. The latter is shown in Fig. 9. The inset shows the finer details of the convergence of $j^1(\lambda_0)$ within the interval $2500 \leqslant \tau_{\max} \leqslant 7000$, revealing that the behavior of the system at $\tau_{\max} < 5000$ still exhibits noticeable deviations from the fixed point, and for safety we have chosen $\tau_{\max} = 10\,000$.

[1] E. Y. Tonkov, *High Pressure Phase Transformations: A Handbook*: Vols. 1–3 (Gordon and Breach, Amsterdam, 1992).

[2] I. Birkby and R. Stevens, Key Eng. Mater. **122–124**, 527 (1996); R. I. Todd and M. P. S. Saran, Transformation toughening, in *Materials Processing Handbook*, edited by J. R. Groza (CRC Press, Boca Raton, FL, 2007), Vol. 20, pp. 1–20.

[3] P. M. Kelly and L. R. F. Rose, Prog. Mater. Sci. **47**, 463 (2002).

[4] The exception is represented by some austenite-martensite transformations exhibiting much broader hystereses.

[5] S. J. Pennycook, Ultramicroscopy **123**, 28 (2012).

[6] S. J. Wang, H. Wang, K. Du, W. Zhang, M. L. Sui, and S. X. Mao, Nature Commun. **5**, 3433 (2014).

[7] S. W. Robertson *et al.*, Acta Mater. **55**, 6197 (2007).

[8] I. Roth *et al.*, in *ESOMAT 2009–8th European Symposium on Martensitic Transformations*, edited by P. Sittner, V. Paidar, and H. Seiner (EDP Sciences, Les Ulis, France, 2009), paper Nr. 06030.

[9] S. Daly *et al.*, Acta Mater. **55**, 6322 (2007).

[10] X. Tan *et al.*, Acta Mater. **62**, 114 (2014).

[11] F. Meschke *et al.*, J. Am. Ceram. Soc. **83**, 353 (2000).

[12] Y. H. Lu *et al.*, Intermetallics **10**, 823 (2002).

[13] S. D. Antolovich and D. Fahr, Eng. Fract. Mech. **4**, 133 (1972); E. Hornbogen, Acta Metall. **26**, 147 (1978).

[14] S. K. Hann and J. D. Gates, J. Mater. Sci. **32**, 1249 (1997); E. C. Oliver *et al.*, Appl. Phys. A **74**, s1143 (2002); Z. Khan and M. Ahmed, J. Mater. Eng. Perform. **5**, 201 (1996); M. K. Banerjee, N. R. Bandyopadhyay, and J. Mazumder, *Processing and Fabrication of Advanced Materials VI* (IOM Communications, London, 1998), Vols. 1 and 2; H. Oettel and U. Martin, Int. J. Mater. Res. **97**, 1642 (2006).

[15] A. L. McKelvey and R. O. Ritchie, Philos. Mag. A **80**, 1759 (2000); Metall. Mater. Trans. A **32**, 731 (2001); H. F. Lopez, Mater. Lett. **51**, 144 (2001); K. Kimura, T. Asaoka, and K. Funami, in *Proceedings of the International Conference on Thermomechanical Processing of Steels and Other Materials* (TMS, Pittsburgh, PA, 1997), Vols. I and II, p. 1675; X. Wang and Z. Yue, in *Fracture and Damage Mechanics V*, Pts 1 and 2, edited by M. H. Aliabadi, Q. Li, L. Li, and F. G. Buchholz (Trans

Tech Publications, Zurich, 2006), Vol. 324-325, p. 919; G. M. Loughran, T. W. Shield, and P. H. Leo, Int. J. Solids Struct. **40**, 271 (2003); H. Qiu *et al.*, Mater. Sci. Eng. A **579**, 71 (2013); U. D. Hangen and G. Sauthoff, Intermetallics **7**, 501 (1999); L. E. Tanner, D. Schryvers, and S. M. Shapiro, Mater. Sci. Eng. A **127**, 205 (1990); A. Paradkar *et al.*, Metall. Mater. Trans. A **40**, 1604 (2009).

[16] M. Kerr, M. R. Daymond, R. A. Holt *et al.*, Scr. Mater. **62**, 341 (2010).

[17] S. O. Kramarov, N. Y. Egorov, and L. M. Katsnel'son, Fizika Tverdogo Tela **28**, 2858 (1986) [Sov. Phys.–Solid State **28**, 1602 (1986)]; A. A. Grekov, Y. V. Dashko, S. O. Kramarov *et al.*, Ferroelectr. Lett. **8**, 59 (1988); C. S. Lynch, R. M. McMeeking, and Z. Suo, in *Second International Conference on Intelligent Materials. ICIM '94* edited by C. A. Rogers and G. G. Wallace (Technomic Publishing Co., Lancaster, PA, 1994), p. 856.

[18] G. G. Siu and W. G. Zeng, J. Mater. Sci. **28**, 5875 (1993).

[19] J. Karger-Kocsis and J. Varga., J. Appl. Polym. Sci. **62**, 291 (1996); J. Karger-Kocsis, J. Varga, and G. W. Ehrenstein, *ibid.* **64**, 2057 (1997); H.-J. Sue, J. D. Earls, and R. E. Hefner, Jr., J. Mater. Sci. **32**, 4039 (1997); S. T. Kim *et al.*, *ibid.* **33**, 2421 (1998); G. A. Maier *et al.*, Macromolecules, **38**, 6099 (2005).

[20] J. A. Horton, J. L. Wright, and J. H. Schneibel, in *Bulk Metallic Glasses*, edited by W. L. Johnson, A. Inoue, and C. T. Liu, Vol. 554 (Cambridge University Press, 1999), pp. 185.

[21] J. A. Donovan, Nippon Gomu Kyokaishi **75**, 239 (2002); S. Trabelsi, P.-A. Albouy, and J. Rault, Macromolecules, **35**, 10054 (2002); H. P. Zhang, J. Niemczura, G. Dennis, K. Ravi-Chandar, and M. Marder, Phys. Rev. Lett. **102**, 245503 (2009); J.-B. Le Cam and E. Toussaint, Macromolecules **43**, 4708 (2010); N. Saintier, G. Cailletaud, and R. Piques, Mater. Sci. Eng. A **528**, 1078 (2011).

[22] E. Sgambittera, C. Maletta, and F. Furgiuele, Scr. Mater. **101**, 64 (2015).

[23] P. R. Okamoto, N. Q. Lam, and S. Ohnuki, J. Electron Microsc. **48**, 481 (1999).

[24] K. Nishimura and N. Miyazaki, Cmes-Computer Modeling in Engineering & Sciences **2**, 143 (2001).

[25] Y.-F. Guo and D.-L. Zhao, Mater. Sci. Eng. A **448**, 281 (2007); Y.-F. Guo, Y.-S. Wang, and D.-L. Zhao, Acta Mater. **55**, 401 (2007).

[26] A. Latapie and D. Farkas, Modell. Simul. Mater. Sci. Eng. **11**, 745 (2003); R. Matsumoto *et al.*, Cmes-Computer Modeling in Engineering & Sciences **9**, 75 (2005) ; I. R. Vatne *et al.*, Mater. Sci. Eng. A **560**, 306 (2013).

[27] M. J. Buehler, H. Tang, A. C. T. van Duin, and W. A. Goddard, Phys. Rev. Lett. **99**, 165502 (2007).

[28] D. Sherman, M. Markovitz, and O. Barkai, J. Mech. Phys. Solids **56**, 376 (2008); F. Atrash and D. Sherman, *ibid.* **60**, 844 (2012).

[29] J. R. Kermode *et al.*, Nature (London) **455**, 1224 (2008).

[30] J. Mei *et al.*, Int. J. Solids Struct. **48**, 3054 (2011).

[31] M. Ruda, D. Farkas, and G. Bertolino, Comput. Mater. Sci. **49**, 743 (2010).

[32] Y. Zhang *et al.*, J. Nucl. Mater. **430**, 96 (2012).

[33] A. Falvo *et al.*, J. Mater. Eng. Perform. **18**, 679 (2009).

[34] B. L. Karihaloo and J. H. Andreasen, *Mechanics of Transformation Toughening and Related Topics* (Elsevier, Amsterdam, 1996).

[35] L. D. Landau and E. M. Lifshitz, *Statistical Physics* (Pergamon, Oxford, 1985).

[36] V. I. Levitas, Int. J. Plasticity **16**, 805 (2000); **16**, 851 (2000); A. V. Idesman, V. I. Levitas, and E. Stein, *ibid.* **16**, 893 (2000).

[37] C. Bjerken and A. R. Massih, arXiv:1110.1292.

[38] A. Boulbitch and A. L. Korzhenevskii, Phys. Rev. E **93**, 063001 (2016).

[39] A. Boulbitch and A. L. Korzhenevskii, Eur. J. Phys. B **89**, 261 (2016).

[40] A. A. Boulbitch and P. Tolédano, Phys. Rev. Lett. **81**, 838 (1998).

[41] A. Boulbitch and A. L. Korzhenevskii, Phys. Rev. Lett. **107**, 085505 (2011).

[42] A. Boulbitch and A. L. Korzhenevskii, Europhys. Lett. **112**, 16003 (2015).

[43] Y. M. Gufan, *Structural Phase Transitions* (Nauka, Moscow, 1983) (in Russian).

[44] J. C. Toledano and P. Toledano, *The Landau Theory of Phase Transitions* (World Scientific, Singapore, 1987).

[45] A. Z. Patashinskij and V. L. Pokrovskij, *Fluctuation Theory of Phase Transitions* (Pergamon, Oxford, 1979).

[46] M. E. Lines and A. M. Glass, *Principles and Applications of Ferroelectrics and Related Materials* (Clarendon, Oxford, 1977).

[47] A. Onuki, *Phase Transitions Dynamics* (Cambridge University Press, Cambridge, UK, 2002).

[48] T. A. Aslanian and A. P. Levanyuk, Solid State Commun. **31**, 547 (1979).

[49] L. P. Pitaevskii, E. M. Lifshitz, and L. D. Landau, *Statistical Physics. Part 2. Theory of Condensed State* (Butterworth-Heinemann, Oxford, 1995).

[50] T. H. Geballe and V. B. Compton, Rev. Mod. Phys. **35**, 1 (1963).

[51] N. Emery, C. Hérold, J. F. O. Marêché, and P. Lagrange, Sci. Technol. Adv. Mater. **9**, 044102 (2008).

[52] T. Rachi *et al.*, Sci. Technol. Adv. Mater. **7**, S88 (2006).

[53] M. Iizumi *et al.*, Phys. Rev. B **15**, 4392 (1977).

[54] V. Dvořák, Phys. Status Solidi B **46**, 763 (1971).

[55] C. Barta, A. A. Kaplyanskii, V. V. Kulakov, B. Z. Malkin, and Yu. F. Markov, ZhETF **70**, 1429 (1976) [JETP **43**, 744 (1976)].

[56] E. S. Larin, Fizika Tverdogo Tela **26**, 3019 (1984) [Sov. Phys.–Solid State **26**, 3019 (1984)].

[57] V. V. Men'shenin, J. Exp. Theor. Phys. **120**, 1019 (2015).

[58] U. Altzmony and M. P. Dariel, Phys. Rev. B **13**, 4006 (1976); U. Altzmony, M. P. Dariel, and G. Dublon, *ibid.* **15**, 3565 (1977).

[59] L. Q. Chen, in *Physics of Ferroelectrics: A Modern Perspective*, edited by K. M. Rabe, C. H. Ahn, and J. M. Triscone (Springer, Berlin, 2007), Vol. 105, pp. 363–371.

[60] Y. Wang, D. Banerjee, C. C. Su, and A. G. Khachaturyan, Acta Materialia **46**, 2983 (1998).

[61] I. L. Kraizman and V. P. Sakhnenko, Pis'ma v ZhETF **40**, 173 (1984) [JETP Lett. **40**, 931 (1984)].

[62] S. A. Brazovskii and I. E. Dzyaloshinskii, Pis'ma v ZhETF **21**, 360 (1975) [JETP Lett. **21**, 164 (1975)].

[63] G. Helgesen, J. P. Hill, T. R. Thurston, and D. Gibbs, Phys. Rev. B **52**, 9446 (1995).

[64] D. Mukamel and S. Krinsky, Phys. Rev. B **13**, 5065 (1976).

[65] P. Toledano and V. Dmitriev, *Reconstructive Phase Transitions in Crystals and Quasicrystals* (World Scientific, Singapore, 1996).

[66] M. Sigrist and H. Monien, J. Phys. Soc. Jpn. **70**, 2409 (2001); Y. A. Ying *et al.* Nat. Commun. **4**, 2596 (2013).

[67] Yu. M. Gufan and V. P. Sakhnenko, Fizika Tverdogo Tela **14**, 1915 (1972) [Sov. Phys.–Solid State **14**, 1660 (1973)].

[68] S. A. Brazovskii, I. E. Dzyaloshinskii, and B. G. Kukharenko, ZhETF **70**, 2257 (1976) [JETP **43**, 1178 (1976)].
[69] E. Bouchbinder *et al.*, Rep. Prog. Phys. **77**, 046501 (2014).
[70] H. Gao, J. Mech. Phys. Solids **44**, 1453 (1996); M. J. Buehler, F. F. Abraham, and H. Gao, Nature (London) **426**, 141 (2003).
[71] A. Karma, D. A. Kessler, and H. Levine, Phys. Rev. Lett. **87**, 045501 (2001); V. Hakim and A. Karma, *ibid.* **95**, 235501 (2005); R. Spatschek, M. Hartmann, E. Brener, H. Muller-Krumbhaar, and K. Kassner, *ibid.* **96**, 015502 (2006).
[72] V. P. Dmitriev, S. B. Rochal, Y. M. Gufan, and P. Toledano, Phys. Rev. Lett. **60**, 1958 (1988); **62**, 844 (1989).
[73] W. A. Wooster, *Tensors and Group Theory for the Physical Properties of Crystals* (Clarendon, Oxford, 1973).
[74] L. D. Landau and E. M. Lifshitz, *Electrodynamics of Continuous Media* (Butterworth-Heinemann, Oxford, 2004).
[75] More complex situations also can be met [43]. In some cases, combinations like $(\eta,0,\ldots)$ and $(-\eta,0,\ldots)$ may correspond to the so-called antiphases. We do not go here into a discussion of such situations and their difference from domains.
[76] We refer the reader to section 121 of the textbook [35] for details.
[77] M. M. Vainberg and V. A. Trenogin, *Theory of Branching of Solutions of Non-Linear Equations* (Noordhoff, Leyden, 1974).
[78] J. D. Eshelby, *Elastic Inclusions and Inhomogeneities* (North Holland, Amsterdam, 1961).
[79] G. P. Cherepanov, *Mechanics of Brittle Fracture* (McGraw-Hill, New York, 1979).
[80] N. Simha and L. Truskinovsky, Acta Metall. **42**, 3827 (1994).
[81] L. T. Latush *et al.*, Ferroelectrics **48**, 247 (1983).
[82] T. Ishidate, S. Abe, H. Takahashi, and N. Mori, Phys. Rev. Lett. **78**, 2397 (1997).
[83] B. Budiansky, J. W. Hutchinson, and J. C. Lambropoulos, Int. J. Solids Struct. **19**, 337 (1983).
[84] A. G. Evans and R. M. Cannon, Acta Metall. **34**, 761 (1986).
[85] L. B. Freund, *Dynamic Fracture Mechanics* (Cambridge University Press, Cambridge, 1998).
[86] M. A. Krivoglaz, *Theory of X-ray and Thermal-Neutron Scattering by Real Crystals* (Plenum, New York, 1969).
[87] See the tables in pp. 889–902 of the book [79].
[88] S. Panteny, C. R. Bowen, and J. Stevens, Mater. Sci. **41**, 3837 (2006); B. Ertug, B. N. Cetiner, G. Sadullahoglu *et al.*, Acta Phys. Pol. A **123**, 188 (2012); R. F. Cook, C. J. Fairbanks, B. R. Lawn, and Y. W. May, J. Mater. Res. **2**, 345 (1987).
[89] H. Vogt, J. A. Sanjurjo, and G. Rossbroich, Phys. Rev. B **26**, 5904 (1982); I. Ponomareva, L. Bellaiche, T. Ostapchuk, J. Hlinka, and J. Petzelt, *ibid.* **77**, 012102 (2008); F. Wan, J. G. Han, and Z. Y. Zhu, Phys. Lett. A **372**, 2137 (2008).
[90] R. Blinz and B. Žekš, *Modes in Ferroelectrics and Antiferroelectrics* (North-Holland, New York, 1974).
[91] J. Jones and M. Hoffman, J. Am. Ceram. Soc. **89**, 3721 (2006).
[92] A different situation takes place in the case of the so-called proper ferroelastics. The latter are, however, rather rare. See, for example, V. P. Sakhnenko and V. M. Talanov, Sov. Phys.–Solid State **21**, 1401 (1979); **22**, 458 (1980). They are outside the scope of this paper. Fizika Tverdogo Tela **21**, 2435 (1979); **22**, 785 (1980).
[93] Wolfram Research, Inc., *Mathematica*, Version 11.0.
[94] S. G. Lekhnitskii, *Theory of Elasticity of an Anisotropic Elastic Body* (Holden-Day, Oakland, CA, 1963).
[95] G. N. Savin, *Stress Concentration Around Holes* (Pergamon, New York, 1961).
[96] E. M. Lifshitz and L. P. Pitaevskii, *Physical Kinetics* (Butterworth-Heinemann, Oxford, 1981), Sec. 101.